Medical & Biological Engineering & Computing (2022) 60:1075–1098
https://doi.org/10.1007/s11517-022-02514-2

ORIGINAL ARTICLE

A multi-layered hybrid model for cancer cell invasion

Sounak Sadhukhan[1] · **P. K. Mishra**[1]

Received: 19 March 2021 / Accepted: 17 January 2022 / Published online: 28 February 2022

Abstract
In this article, a hybrid model is developed based on multi-scale concept for solid tumour cell invasion into a healthy tissue. Our aim is to study the tumour heterogeneity due to the geometry of a growing tumour caused by the phenotypic transformations of cells. In this context, an early vascular growth is considered after angiogenesis. Hence, the microenvironment of the solid tumour is rich of oxygen and nutrients. It is also considered that epidermal growth factor (EGF) is distributed into the surrounding extracellular matrix (ECM) of the tumour. The developed multi-layered model consists of three layers: intracellular or subcellular, cellular, and extracellular or tissue layer. The model integrates the events that occur simultaneously in these three layers to identify the underlying diversity. Here, every cell is represented as an agent. Characteristics of an agent are controlled by its intracellular protein expressions and its surrounding microenvironment. A mature proliferative or migratory or hybrid cell agent spawn two indistinguishable children unless it may convert into other phenotype due to influence of the microenvironment. Further, a simple cell cycle model is adapted which is influenced by EGF-EGFR signalling pathway and the external oxygen and nutrients. Moreover, migratory and hybrid cells secrete several matrix degrading enzymes (MDEs) which remodel the ECM for tumour invasion locally. Several biomechanical forces are considered that simultaneously act on the cancer cells. The outcome of the model is very similar to the results reported in earlier studies. The model shows the characteristics of cancer invasion that include sustainable proliferation by ignoring growth suppressor signals and reproduction of cancer cells at abnormal proportion, restrict apoptosis, and invade into the surrounding tissue. As the simulation parameters get modified due to different biochemical and biophysical processes, the robustness of the model is determined. It is found that only a number of proliferative cells are moderately sensitive to the parameters and others are less-sensitive.

Keywords Multi-scale model · EGF-EGFR signalling pathway · Agent-based model · Cancer cell invasion

1 Introduction

During the avascular phase, tumour growth is restricted due to inadequate nutrient and oxygen supply [10, 33, 74]. To sustain its growth, tumour cells secrete several biochemical species (tumour angiogenic factors (TAFs)) which stimulate the endothelial cells of the nearby blood vessels. New capillary sprouts are formed from the stimulated endothelial cells during this phase. Capillary sprouts move in the direction of tumour due to the higher concentration of the TAFs. These capillaries are often fused to form loops to build a complex vascular network. This pathological phenomenon is known as angiogenesis.

During angiogenesis, tumour cells access the blood vessels directly (vascular phase) and take oxygen, nutrients, and growth factors without any restrictions. In the vascular phase, cancer cells secrete several MDEs, mainly diffusible matrix metalloproteinase-2 (MMP-2) [37] and membrane-bounded membrane type-1 MMP (MT1-MMP) [64] which help to remodel the ECM [7]. The ECM is constructed with a complex mixture of macromolecules (MMs) like collagen, laminin, fibronectin, and vitronectin [57]. Among these MMs, collagen is required for maintaining the structural integrity, and others are crucial for cellular adhesion, cell spreading, and cell motility. These MMs are bounded within the tissue (non-diffusible). Degradation of the ECM is an important event during invasion-metastatic cascade [42].

✉ Sounak Sadhukhan
sounaks.cse@gmail.com

P. K. Mishra
mishra@bhu.ac.in

[1] Department of Computer Science, Institute of Science, Banaras Hindu University, Varanasi 221005, India

Also, the expanding tumour creates a huge biophysical pressure on the surrounding tissues. As a result, tumour gets extra spaces for expansion, and it grows in volume abruptly. During this phase, tumour cells invade into the neighbouring tissues along the least resilient path through the ECM (invasion).

Further, tumour cells may invade into the surrounding blood and/or lymphatic vessels by getting separated from the primary tumour singly or collectively (intravasation) [72]. Blood and/or lymphatic vessels help the invaded tumour cells to circulate any sites of the body. But this task is not very easy. To survive and proliferate in the new environment, tumour cells are transformed that helps them to adapt new conditions and keep them alive. The circulated tumour cells which survived within the vessels may often get stuck to the vascular endothelium of distant organs (extravasation) and develop new colonies of cells (metastasis) [72]. Statistical analysis shows that 90% of cancer patients die of metastasis [29].

Tumour cell migration and invasion into the other organs or blood/lymphatic vessels are the pillars of metastasis. There can be various ways of cancer cell migration depending on cell types and the degrees of differentiation. The main cause of these mechanisms is the dynamic reformations of actin cytoskeleton that produces the necessary forces for cancer cell migration. During epithelial cell differentiation, the utility of cadherin is inhibited which leads to retraction of the cell-cell adhesion. The suppression of the cell-cell adhesive force separates the tumour cells from each other and makes them ready for solitary or collective migration [44]. This event is called epithelial-to-mesenchymal transition (EMT). E-cadherin is the key element of epithelial adherens junctions. Due to the reduction of E-cadherin in mesenchymal cell-cell junctions during EMT, N-cadherin increases (cadherin switch), thereby leading to cell motility and invasion [40]. This functional loss can happen due to abnormality in chromosomes, mutations in germline and somatic genes, DNA hyper-methylation of E-cadherin gene (Cdh1), transcriptional repression, signal transduction of a huge number of growth stimuli, and Notch signalling. Numerous growth stimuli like, hepatocyte growth factor, fibroblast growth factors (FGF), EGF, transforming growth factor β (TGF-β), and Notch signalling stimulate the E-cadherin loss. Also, hypoxic conditions in tumour cells influence the cells for migration and spreading.

In general, EMT is considered as a transformation process that alters more epithelial cells into more mesenchymal phenotype [50, 21]). Another process exists in the phenomena which are just reverse to EMT, i.e. mesenchymal-to-epithelial transition (MET) [60]. MET reverses the phenotypic changes induced by the EMT. Recently, researchers [50] have found that a new cell line exists along with more epithelial and more mesenchymal phenotypes. They also observed that this new type of cells carries the features of the epithelial as well as mesenchymal cells. Researchers named this phenotype a hybrid/partial state. More epithelial-type cells are more proliferative and less motile, while more mesenchymal-type cells are more motile but less proliferative. Recent studies show that mesenchymal cells may have full cell cycle arrest during the cell cycle [43, 68], while the hybrid cells are proliferative as well as motile [30].

Motile tumour cells may breach the lymphatic and/or blood vessel wall and then reach to other sites of the body through the lymphatic (lymphatic spread) and/or blood vessels (haematogenous spread). Motile tumour cells move either singly or collectively, and these movements are simultaneous. On the other hand, single cell motility is classified into mesenchymal cell migration and amoeboid migration [25]. Either or both of them can be seen in cancer cells. Collective cell migration preserves their cell-cell junctions and move with the connection to their originating tissue or separately in the form of a sheet, strands, tubes, and clusters. Migrating cells develop a cone or finger-like cell membrane bulge and then intravasate and circulate like cell clusters that are very proficient in embolizing lymphatic or blood vessels. Collective migration needs synchronization between cell-cell adhesion and cell contractibility [48]. It can be seen in breast cancer, prostate cancer, lung cancer, melanoma, etc. Motile cells collectively infiltrate the surrounding matrix. The leading cell generates an invasion path using β1-integrin-mediated focal adhesions and metalloproteinases to rupture the collagen fibres. It forms a tube-like structure in which the following cells can migrate. Invasive migration and proteolytic matrix remodelling control the collective cell motility.

Cancer cells interact with its surrounding environment in bi-directional way. It not only affects the surrounding microenvironment but also involve the stroma and other noncancerous cells for invasion and metastasis [71]. These complex interactions are very difficult to understand in biological wet-lab experiments. Mathematical models are used widely to explore this complex phenomenon which can help in clinical diagnostics and therapeutics. Over the last two decades, researchers have developed several mathematical models from different perspectives to understand various complexities in solid tumour invasion and metastasis. Anderson et al. [4] have described a macro-scale mathematical model for cancer cell invasion based on partial differential equations (PDEs). The model consists of tumour cells that secrete MDEs for degenerating the host tissues. The model assumes the tumour as a single entity. A series of PDEs describe the activation of MDEs, remodelling of the ECM, and the migratory response of the tumour. Numerical results are also compared with the clinical observations qualitatively. A simple tri-phasic multicellular model is described by Ambrosi and Preziosi [2] which considered that the motility of cells

is due to cell-cell interactions. The model is also assumed that the biomechanical pressure inside the tumour spheroid and at the edge of external tissue is due to the uncontrolled growth of tumour cells. Chaplain and Lolas [11, 12] have proposed reaction-diffusion-based mathematical models for tumour cell invasion into the tissue to observe the tumour growth dynamics due to the influence of spatiotemporal dynamics of plasminogen activators (PAs). The models show the complex dynamics related to tumour heterogeneity, cancer cell evolution, and invasion.

Gerisch and Chaplain [27] have illustrated the cancer cell invasion model. They have considered cell-cell and cell-matrix adhesion forces. They formulated a sequence of PDEs in which the cells use sensing radius to identify their microenvironment. The paper showed that the nearest cells converge with reaction-diffusion–taxis equations. Sherratt et al. [65] have extended the concept of cell-cell and cell-matrix adhesion to incorporate into the continuum model in which the integral part represented the local microenvironment of a cell. They have used this concept to observe the roles of cell-cell adhesion in cell aggregation. The model described that there exists an equilibrium between cell-cell and cell-matrix adhesion during invasion. Andasari et al. [3] have analysed the roles of urokinase PA (uPA) using a spatiotemporal continuum model which consists of uPA, uPA-inhibitors, plasmin, and the host tissue. Chaplain et al. [13] have developed a mathematical model for cancer cell invasion in which tumour cells invade into the ECM by secreting the MDEs. They have examined cell-cell and cell-matrix bindings in tumour invasion using integral terms.

Deakin and Chaplain [18] have designed a computational model of tumour cell invasion to investigate the effectiveness of soluble, diffusible MMP-2, and membrane-bounded MT1-MMP. In this context, they have considered MMP-14 (activator of MMP-2), the tissue inhibitor metalloproteinases-2, and the porous architecture of the ECM including collagen fibres. They have shown that during the movement through the ECM, cancer cells depend more on membrane-bounded MMPs to forge a path through which degradation by the other MMPs. Domschke et al. [20] have illustrated the spatiotemporal dynamics of cancer cell invasion by accounting cell-cell and cell-matrix adhesion using a continuum model. They have investigated the change in adhesive properties among cancer cell populations during cell growth and the development through time-dependent adhesion characteristics. Their results established a range of heterogeneous dynamics which is similar to tumour invasive growth patterns. Franssen et al. [24] have presented a multi-grid, spatiotemporal model to describe cancer cell invasion as well as metastasis in a single framework. Here, they have shown the spatiotemporal growth of mesenchymal and epithelial cells and their interaction with the ECM. Similar to the work of Deakin and Chaplain [18, 24] also has considered the effects of MMP-2 and MT1-MMP. They have encountered the crucial events of invasion-metastasis cascade by including single-cell and multi-cell invasion, the ECM degradation due to MDEs, intravasation of these motile cells through the leaky blood vessels, circulation of cancer cells into the vessels, and extravasation and metastatic growth of survived circulating tumour cells at the secondary organs. In another study, Franssen and Chaplain [23] have extended their previous work and presented a trade-off between the motile and proliferative phenotype. Here, they have included a mixed phenotypic state with more proliferative and more motile cells. In this model, cancer cells may transit in between these two extreme states through the EMT and the MET. They have also included the likelihood of spread of cancer cells into several distant organs and the microenvironment and immune response at the secondary sites.

Tumour growth and its progression is very complex, multi-layered, and multi-phases dynamical process. In multi-scale tumour microenvironment systems, alterations in any layer lead to spread its effects to the other layers. Therefore, for better underlying biological knowledge about tumour cell invasion, it is required to know the events at different spatiotemporal scales. This is only possible by using the multi-scale modelling approach. There are very few literatures available that focused on the development of multi-scale models for tumour cell invasion into the tissue. In this context, Athale et al. [5] have built a multi-layered spatiotemporal hybrid framework by including an EGF-EGFR network and a mitosis-associated response pathway that decides whether a cell should proliferate or migrate. They have concluded that the behavioural choices in the cellular layer are influenced by its microenvironment. Zhang et al. [75] have extended their previous work [5] and built a novel 3D multi-layer model for simulating brain tumour by including an EGFR protein interaction network with a basic cell cycle model. They have shown that the number of migratory and proliferative cells oscillates over time and also influences the spatiotemporal dynamics of tumour growth. But both of these studies ignore cellular adhesion and chemotactic and haptotactic movements. Rocha et al. [56] have developed a multi-scale hybrid tumour growth model that accounts several biophysical forces acted on the tumour cells. Phenotypic transitions of cellular agent are described that is led by the EGF-EGFR signalling. The EGF-EGFR signalling pathway is modelled with a sequence of ordinary differential equation (ODEs). The data between the cellular and the tissue scale is transferred in both directions through the reaction and source terms of PDEs.

Most of the literatures described above have not considered the effect of physical forces acted on tumour cells during tumour cell invasion, especially most of them have ignored cell-cell adhesion (except Anderson et al. [4], Gerisch and Chaplain [27, 65], and Rocha et al. [56]). Also

most of the researches have considered that cell cycle duration is a fixed time interval (except Zhang et al. [75]). But biologically, cell cycle period may vary depending on the microenvironment. In this article, a multi-layered hybrid model for solid tumour invasion (in epithelial tissue) into the surrounding tissue is developed by incorporating sub-cellular, cellular, and tissue-layer events. The model includes several physical forces like cell-cell adhesion, repulsion, chemotaxis, and haptotaxis. An age-structured cell cycle model is also incorporated with EGF-EGFR pathway that describes the effects of microenvironment on cell division. ABM is one of the modelling techniques that naturally suitable for multi-scale tumour growth modelling. These hybrid models consist of self-governing choice making elements that can be integrated with the systems of ODEs and PDEs. Here, every autonomous cellular agent independently evaluates its situation and makes decisions on the basis of the set of rules.

In this context, we assume that the tumour passes through its avascular and angiogenesis phase. Hence, without the loss of generality, we assume that the microenvironment of the tumour is oxygen and nutrients rich. The vascular tumour initially contains proliferative, hypoxic, quiescent, necrotic, and apoptotic cells. These cells may transform into other phenotypes because of its microenvironment and internal signals. Moreover, we consider that EGF is randomly distributed into the surrounding ECM of the tumour. The alteration of phenotypes is depended on the cell cycle integrated EGF-EGFR signalling pathway, as well as its neighbourhood. The model considers that the mature proliferative or motile or hybrid tumour cells spawn two indistinguishable offspring. Initially these offspring are quiescent. If the microenvironment is suitable for them, then these daughter cells always become like its parent. But if the microenvironment is not supportable, then it can be transformed into any other phenotype depending on its external conditions.

At the subcellular level, cell fates are decided by the EGF-EGFR protein pathway. It decides whether a proliferative cell remains proliferative or transforms into migratory or hybrid phenotype. Cell cycle is regulated by several kinds of sub-cellular species like PLCγ, ERK, cyclin, cyclin-dependent kinases (CDKs), cadherin-1 (Cdh-1), nutrients, and oxygen. Generally, rate of changes in PLCγ and ERK have decided that whether a cancer cell be a proliferative or migratory or hybrid category phenotype. On the other hand, the higher concentration level of p27 converts a proliferative, migratory, or hybrid tumour cell into hypoxic one. Generally, the expression of p27 is very low in cancer cells. But, hypoxic condition overexpresses p27 in the tumour cells. Raise of p27 is responsible for alteration of state of a cancer cell. The hypoxic cell converts into necrotic after a certain time. In this article, an age-structured ODE-based model is incorporated for cell cycle with EGF-EGFR signalling pathway. Here, we consider that p27 inhibits p53 gene expression (growth suppressor signal).

Here, we consider the existence of mixed phenotypic state with more proliferative, more motile, apoptotic, hypoxic, quiescent, and necrotic cells. In this model, cancer cells may transit in between these two extreme states (proliferative and motile) through the EMT and the MET. The tumour cells and its surrounding microenvironment create numerous biomechanical forces that act on the tumour cells and support them to travel through the ECM without any restrictions. These forces perform a key role in tumour cell invasion and metastatic cascade. The model also adapt that membrane-bounded MT1-MMP and the diffusible MMP-2 are the main actors for degrading the ECM. The extracellular activities can be described with a series of PDEs.

Activities in the subcellular, cellular, and extracellular layers are integrated with the agent-based modelling (ABM) which act as a single dynamical system. A graphical version of this model is illustrated in Fig. 1. Aim of this article is to study the tumour cell heterogeneity due to the geometrical change of a growing tumour caused by the phenotypic transformations of cells. The outcome of the model is very similar to the reported results in earlier studies [14, 70, 75]. As the simulation parameters get modified due to different biochemical and biophysical processes, the robustness of the model is determined. The robustness model is established with sensitivity analysis. The model also illustrates the crucial features of the invasive cancer.

This article is organized as follows: Section 2 illustrates the model of subcellular layer that is represented by a couple of ODEs; Section 3 describes the model of cellular layer; Section 4 shows the extracellular layer model that is characterized by a set of PDEs; Section 5 integrates of all the activities across different spatiotemporal layers and computes the simulations of this model with diverse initial conditions; Section 6 establishes robustness of the model using sensitivity analysis; and Section 7 concludes this article.

2 Subcellular layer

Cell is the main functional unit in multicellular environment. Every cell is wrapped within a porous cell membrane. The functions of cell membrane are to guard a cell from the outside environment, maintain its pH level and other molecules in stable condition, etc. Experimental evidence shows that the EGF-EGFR signalling pathway is one of the existing pathways that involved in many types of tumour growth, invasion, and metastasis like breast tumour [47], brain tumour Chicoine and Silbergeld [15], and non-small

lung tumour [28, 34]. Hence, researchers have studied EGF-EGFR pathway extensively to understand the downstream effects which influence the prototypic transformations in tumour cells. Extracellular EGF protein binds with the cellular EGFR [53, 58] that upregulate the EGFR expression in the cancerous cell which increases cell motility and invasiveness and finally raises the chance of metastasis [52, 52].

In this section, the EGF-EGFR signalling pathway model [70] is discussed in brief. A simple age-structured cell cycle model in the context of tumour cell invasion is also incorporated.

2.1 EGF-EGFR protein network model

EGF-EGFR signalling pathway is very complex, multifunctional, and diverse [28]. In the last couple of decades, researchers have studied EGFR-related signalling pathway extensively Brightman and Fell [8, 31, 38, 54, 62, 63, 70], and [32] for the invasive tumour growth modelling. In this research, we have adopted a kinetic model proposed by Wang et al. [70], which contains twenty molecular species (Fig. 2) interacting with each other. In this context, it is assumed that the cellular EGFR pathway is activated by the binding with EGF molecules that scatter surrounding the ECM. The EGF-EGFR signalling pathway includes EGF receptor (EGFR) (Z_2) and non-receptors like PLCγ (Z_6), protein kinases C (PKC) (Z_{11}), Raf (Z_{13}), mitogen-activated protein kinases (MEK) (Z_{15}), and ERK (Z_{18}). Scientists have found the evidence that PLCγ and ERK are the especially responsible for the phenotype transformations of tumour cells [70].

The kinetic model of this signalling pathway consists of twenty ODEs. The model considers that the rate of changes of every molecular species with respect to time is equal to the difference between the net productions and the net consumptions (described in Equation (1)). In Equation (1), Z_i represents the molecular species where $i = 1, 2, \ldots, 20$. Every protein interaction is characterized by u_j where $j = 1, 2, \ldots, 19$ (Fig. 2). Model parameters and the ODEs are defined in Tables 1 and 2, respectively.

$$\frac{d(Z_i)}{dt} = \sum u_{\text{production}} - \sum u_{\text{consumption}} \tag{1}$$

2.2 Cell cycle model

Here, a simple cell cycle model is adapted. It is also modified as required to fit in the multi-scale environment [59]. The cell cycle is controlled by cyclin, CDKs, APC, surrounding nutrients, and oxygen. The actions of cyclin-CDK are supressed by the over-expression of p27 gene. This event delays the advancement of cell cycle. Further, cyclin-CDK stimulates the retinoblastoma (RB) protein (Fig. 2).

The model assumes that the p27 expression decides whether a cell converts from proliferative or migratory or hybrid cell to a hypoxic cell or not. Hypoxic cells transform into necrotic after a certain moments. Moreover, it assumes that nutrients and oxygen work as suppressors of p27 and activators of cyclin-CDK (Fig. 2). Here we consider that cell cycle controls its mass (m) and radius (R).

Changes in Cdh1-APC (Z_{21}), cyclin-CDK (Z_{22}), p27 (Z_{23}), nPRB (Z_{24}), p53 (Z_{25}), R, and m are described with the following ODEs:

$$\frac{d(Z_{21})}{dt} = \frac{1 + k_{20}.Z_{24}}{K_{20} + 1 - Z_{21}} - \frac{k_{21}R.Z_{21}.Z_{22}}{K_{21} + Z_{21}} \tag{2}$$

$$\frac{d(Z_{22})}{dt} = k_{22}\frac{(1 + \alpha.C_O.C_N).C_O.C_N}{K_{Z_{22}} + C_O.C_N} - (k_{23} + k_{24}.Z_{21} + k_{25}.Z_{23}).Z_{22} \tag{3}$$

$$\frac{d(Z_{23})}{dt} = k_{26} - k_{27}\frac{C_O.C_N}{K_{Z_{23}} + C_O.C_N}.Z_{23} \tag{4}$$

$$\frac{d(Z_{24})}{dt} = k_{28} - (k_{29} + k_{28}.Z_{22}).Z_{24} \tag{5}$$

$$\frac{d(Z_{25})}{dt} = k_{30} - k_{31}\frac{Z_{23}}{K_{Z_{25}} + Z_{23}}.Z_{25} \tag{6}$$

$$\frac{dm}{dt} = k_{32}.m.\left(1 - \frac{m}{m_*}\right) \tag{7}$$

$$\frac{dR}{dt} = k_{33}.R.\left(1 - \left(\frac{R}{R_*}\right)^3\right) \tag{8}$$

In Equations (2-8), Z_{21}, Z_{22}, Z_{23}, Z_{24}, and Z_{25} are the kinetic parameters; $k_{20} - k_{33}$,$K_{Z_{22}}$,$K_{Z_{23}}$, $K_{Z_{24}}$, and α are the dimensionless constant (DCs). The value of α varies depending on the phenotype of cancer cells. It is considered that if cell is more proliferative, then $\alpha = 0.9$; if the cell is more motile, then $\alpha = 0.3$; and for hybrid cells $\alpha = 0.6$. In Eq. (2), K_{20} and $K_{21} << 1$ (Michaelis-Menten constants). In Eqs. (7–8), m_* and R_* are characterized as the mass and radius of a mature proliferative cell, and they are in ng and μm scale. C_O and C_N in Equations (2-3) are represented surrounding oxygen and nutrient levels (dimensionless). We assume that cell division would occur if Z_{21} is below the threshold Z_{21}^{th} and Z_{22} is above the threshold Z_{22}^{th}. Here, it is considered that $Z_{21}^{th} = 0.004$ and $Z_{22}^{th} = 0.05$ [1]. We consider that 'G1' phase

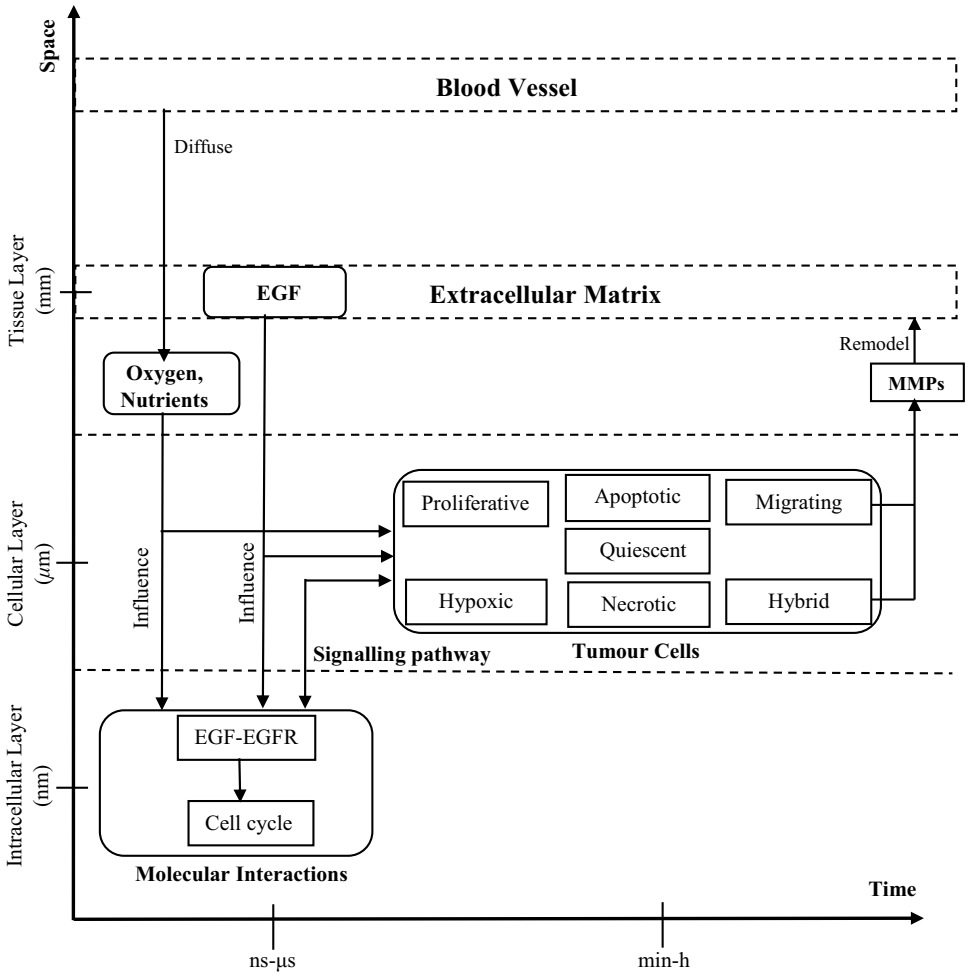

Fig. 1 Multi-layered hybrid framework for solid tumour cell invasion.

in cell cycle continues until the concentration of $Z_{21} > Z_{22}$, whereas during the other phases $Z_{22} > Z_{21}$.

The system of equations for the intracellular model is described in Tables 1, 2, and Equations (2-8). Fourth-order Runge-Kutta method has been used to solve the ODEs with the values mentioned in Table 3 and step size t_{mol}. It is found that the mean cell cycle duration is 23.86 ± 7.76h (in simulation). The preliminary values required to solve these ODEs (Eqs. (2-8)) are as follows [59]:

$$Z_{21} = 0.9; Z_{22} = 0.01; Z_{23} = 0.0; Z_{24} = 1.0; Z_{25} = 0.0; m = \frac{m_*}{2}; \text{and } R = \frac{R_*}{2}$$

3 Cellular layer model

The intracellular and extracellular processes directly effect on tumour cell phenotype. A cell may have several number of mutations in cell cycle duration that depend on the intracellular as well as tissue layer. These repeated mutations may lead to phenotype transformations. It is also considered that at the cellular layer, tumour cells are experienced different biophysical forces that move cancer cells in the ECM freely.

Here, we describe the phenotype alterations in cancer cells and the applied forces on cancer cells.

3.1 Cancer cell phenotype transition

Here, we consider that a cancer cell could be one of the phenotypes in P_s= {'P', 'H', 'Q', 'A', 'N', 'M', 'Hy'} in its life time. Here, 'P', 'Q', 'H', 'A', 'N' 'M', and 'Hy' denote the proliferative, quiescent, hypoxic, apoptotic, necrotic, migratory, and hybrid state respectively. In this research, we have considered that every proliferative, migratory, and hybrid cancer cells are in quiescent state initially. Due to external microenvironment and internal protein expressions, a tumour cell transforms from its current state to another state, or it may remain same. Hence, phenotype of a cancer cell at the next time instance depends on the current state and its subcellular as well as the extracellular

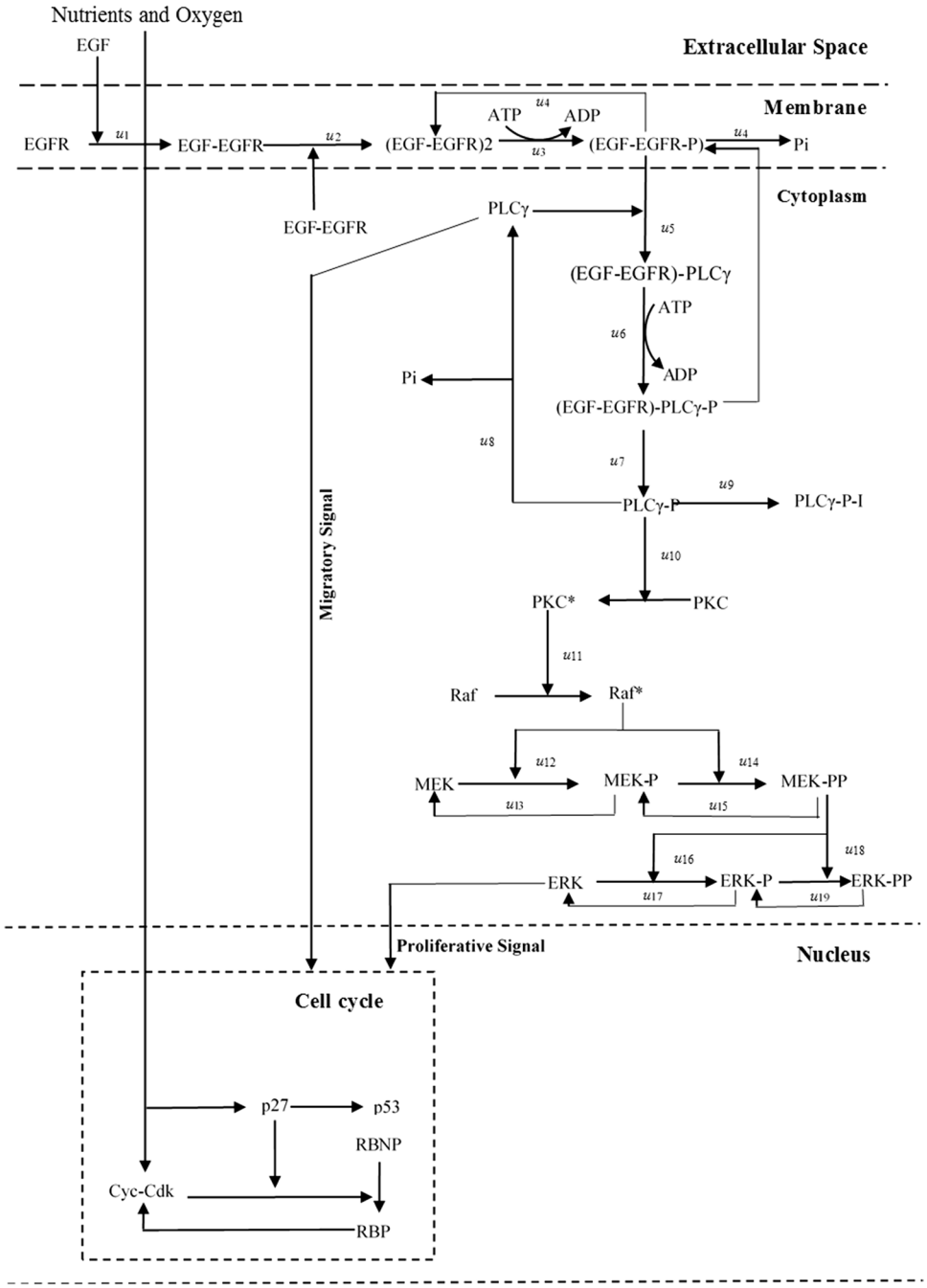

Fig. 2 Kinetic model EGF-EGFR signalling pathway with a simple cell cycle model. The arrows represent the influential signal.

conditions. The state transition diagram of cancer cell is presented in Fig. 3.

A proliferative cancer cell may alter into other phenotypes ('H', 'M', or 'Hy'), or it remains proliferative unless it divides into two offspring after becoming adult. Absence of mitogenic stimuli in the early phase of the cell cycle, new offspring stuck into 'G0' phase and they become quiescent. Hence, in this article, it is considered that offspring are in quiescent state initially and its state may change in future depending on its niche. A quiescent cell i may transform into proliferative state if its parent (Pa(i)) was in proliferative state and the surrounding microenvironment is suitable. Suitable microenvironment refers to sufficient nutrients ($C_N > \lambda_N^P$) and oxygen ($C_O > \lambda_O^P$) that is required for cell proliferation. Therefore, the probability (P_1) for the transition from 'Q' to 'P' depends on available nutrients and oxygen. Hence, P_1 is defined as (Eq. (9))

Table 1 Kinetic equations and initial conditions [70]

Reactant	Molecules	Initial condition (in [nM])	Kinetic equation
Z_1	EGF	Tissue Scale EGF	$d(Z_1)/dt = -u_1$
Z_2	EGFR	80	$d(Z_2)/dt = -u_1$
Z_3	EGF-EGFR	0	$d(Z_3)/dt = u_1 - 2u_2$
Z_4	(EGF-EGFR)2	0	$d(Z_4)/dt = u_2 + u_4 - u_3$
Z_5	EGF-EGFR-P	0	$d(Z_5)/dt = u_3 + u_7 - u_4 - u_5$
Z_6	PLC_γ	10	$d(Z_6)/dt = u_8 - u_5$
Z_7	EGF-EGFR- PLC_γ	0	$d(Z_7)/dt = u_5 - u_6$
Z_8	EGF-EGFR- PLC_γ-P	0	$d(Z_8)/dt = u_6 - u_7$
Z_9	PLC_γ-P	0	$d(Z_9)/dt = u_7 - u_8 - u_9 - u_{10}$
Z_{10}	PLC_γ-P-I	0	$d(Z_{10})/dt = u_9$
Z_{11}	PKC	10	$d(Z_{11})/dt = -u_{10}$
Z_{12}	PKC*	0	$d(Z_{12})/dt = u_{10} - u_{11}$
Z_{13}	Raf	100	$d(Z_{13})/dt = -u_{11}$
Z_{14}	Raf*	0	$d(Z_{14})/dt = u_{11} - u_{12} - u_{14}$
Z_{15}	MEK	120	$d(Z_{15})/dt = u_{13} - u_{12}$
Z_{16}	MEK-P	0	$d(Z_{16})/dt = u_{12} + u_{15} - u_{13} - u_{14}$
Z_{17}	MEK-PP	0	$d(Z_{17})/dt = u_{14} - u_{15} - u_{16} - u_{18}$
Z_{18}	ERK	100	$d(Z_{18})/dt = u_{17} - u_{16}$
Z_{19}	ERK-P	0	$d(Z_{19})/dt = u_{16} + u_{19} - u_{17} - u_{18}$
Z_{20}	ERK-PP	0	$d(Z_{20})/dt = u_{18} - u_{19}$

$$P_1\left(\mathrm{P_S}(t+\Delta t) =' \mathrm{P}' | \mathrm{P_S}(t) =' \mathrm{Q}' \wedge \mathrm{Pa}(i) =' \mathrm{P}'\right) = 1 - \exp\left[-\left(\frac{C_\mathrm{N} - \lambda_\mathrm{N}^\mathrm{P}}{\lambda_\mathrm{N}^\mathrm{P}}\right)\left(\frac{C_\mathrm{O} - \lambda_\mathrm{O}^\mathrm{P}}{\lambda_\mathrm{O}^\mathrm{P}}\right)\right] \tag{9}$$

A motile or hybrid tumour cell may also have transformed into a proliferative cell if condition C_3 (is discussed later) has satisfied.

A proliferative, motile or hybrid cancer cell may transform into hypoxic state, if p27 protein overexpress than a predefined level $[\mathrm{p27}]_{th}^{\mathrm{H}}$ because of lack of oxygen and nutrients. Here, we assume that cancer cells which are in hypoxic state are suspended from its cell cycle. The chances for the transition from 'P' to 'H' (P_2), 'M' to 'H' (P_3), and 'Hy' to 'H' (P_4) are defined in Equations (10-12), respectively,

$$P_2\left(\mathrm{P_S}(t+\Delta t) =' \mathrm{H}' | \mathrm{P_S}(t) =' \mathrm{P}'\right) = 1 - \exp\left(\frac{[\mathrm{p27}] - [\mathrm{p27}]_{th}^{\mathrm{H}}}{[\mathrm{p27}]_{th}^{\mathrm{H}}}\right) \tag{10}$$

$$P_3\left(\mathrm{P_S}(t+\Delta t) =' \mathrm{H}' | \mathrm{P_S}(t) =' \mathrm{M}'\right) = 1 - \exp\left(\frac{[\mathrm{p27}] - [\mathrm{p27}]_{th}^{\mathrm{H}}}{[\mathrm{p27}]_{th}^{\mathrm{H}}}\right) \tag{11}$$

$$P_4\left(\mathrm{P_S}(t+\Delta t) =' \mathrm{H}' | \mathrm{P_S}(t) =' \mathrm{Hy}'\right) = 1 - \exp\left(\frac{[\mathrm{p27}] - [\mathrm{p27}]_{th}^{\mathrm{H}}}{[\mathrm{p27}]_{th}^{\mathrm{H}}}\right) \tag{12}$$

Moreover, a quiescent cell transforms into hypoxic state depending on the nutrients (C_N) and oxygen (C_O) unavailability. If nutrients and oxygen concentration reduces below a certain levels, i.e. $C_\mathrm{N} < \lambda_\mathrm{N}^\mathrm{Q}$, and $C_\mathrm{O} < \lambda_\mathrm{O}^\mathrm{Q}$, then chances for the conversion from 'Q' to 'H' (P_5) rises. Hence, P_5 is defined as (Eq. (13))

$$P_5\left(\mathrm{P_S}(t+\Delta t) =' \mathrm{H}' | \mathrm{P_S}(t) =' \mathrm{Q}'\right) = 1 - \exp\left[-\left(\frac{\lambda_\mathrm{N}^\mathrm{Q} - C_\mathrm{N}}{\lambda_\mathrm{N}^\mathrm{Q}}\right)\left(\frac{\lambda_\mathrm{O}^\mathrm{Q} - C_\mathrm{O}}{\lambda_\mathrm{O}^\mathrm{Q}}\right)\right] \tag{13}$$

Further, a mature/adult proliferative or migratory or hybrid cell divides into two offspring. These two new born cells are characteristically same. They have same mass ($m_*/2$) and consist of same radius ($R_*/2$). These cells are initially quiescent (according to our assumption) and occupy nearby random positions. It is assumed that the point of a parent cell be (x_0, y_0). Then locations of these offspring (quiescent cells) are

$$\left.\begin{aligned} x_1 &= x_0 + R_* \cos\varphi_1;\ \mathrm{y}_1 = y_0 + R_* \sin\varphi_1; \\ x_2 &= x_0 - R_* \cos\varphi_2;\ \mathrm{y}_2 = y_0 - R_* \sin\varphi_2; \end{aligned}\right\} \tag{14}$$

where (x_1, y_1) and (x_2, y_2) are the locations of two offspring; $\varphi_1, \varphi_2 \in [0, 2\pi)$ with uniform distribution. Apoptosis describes programmed cell death. In tumour microenvironment, chances of apoptosis are very low. Therefore, in this paper, we assume that a 'Q' cell may alter into 'A' with the probability (P_6) that is influenced by the number of neighbouring 'Q' cells (n_Q) and the time period it spends as 'Q' (T_Q) cell. Therefore, P_6 is defined as (Eq. (15))

Table 2 Kinetic parameters. Concentrations and the Michaelis-Menten constants (K) are given in [nM]. First and second order rates are given in [s-1] and [nM-1s-1], respectively, and a's are given in [nMs-1] [56]

Reaction	Equations	Kinetic parameters	
u_1	$w_1Z_1Z_2 - w_{-1}Z_3$	$w_1 = 0.003$	$w_{-1} = 0.06$
u_2	$w_2Z_3Z_3 - w_{-2}Z_4$	$w_2 = 0.01$	$w_{-2} = 0.1$
u_3	$w_3Z_4Z_3 - w_{-3}Z_5$	$w_3 = 0.01$	$w_{-3} = 0.1$
u_4	$a_4Z_5/(K_4+Z_5)$	$w_4 = 450.0$	$K_4 = 50.0$
u_5	$w_5Z_5Z_6 - w_{-5}Z_7$	$w_5 = 0.06$	$w_{-5} = 0.2$
u_6	$w_6Z_7 - w_{-6}Z_8$	$w_6 = 1.0$	$w_{-6} = 0.05$
u_7	$w_7Z_8Z_6 - w_{-7}Z_5Z_7$	$w_7 = 0.3$	$w_{-7} = 0.006$
u_8	$a_8Z_9/(Z_8+Z_9)$	$a_8 = 1.0$	$K_8 = 100.0$
u_9	$w_9Z_9 - w_{-9}Z_{10}$	$w_9 = 1.0$	$w_{-9} = 0.03$
u_{10}	$w_{10}Z_9Z_{11} - w_{-10}Z_{12}$	$w_{10} = 0.214$	$w_{-10} = 5.25$
u_{11}	$a_{11}Z_{12}Z_{13}/(K_{11}+Z_{13})$	$a_{11} = 4.0$	$K_{11} = 64.0$
u_{12}	$a_{12}Z_{14}Z_{15}/(K_{12}(1+Z_{16}/k_{14})+Z_{15})$	$a_{12} = 3.5$	$K_{12} = 317.0$
u_{13}	$a_{13}Z_{16}/(K_{13}(1+Z_{17}/K_{15})+Z_{16})$	$a_{13} = 0.058$	$K_{13} = 2200.0$
u_{14}	$a_{14}Z_{14}Z_{16}/(Z_{14}(1+Z_{15}/K_{12})+Z_{16})$	$a_{14} = 2.9$	$K_{14} = 317.0$
u_{15}	$a_{15}Z_{17}/(Z_{15}(1+Z_{16}/K_{13})+Z_{17})$	$a_{15} = 0.058$	$K_{15} = 60.0$
u_{16}	$a_{16}Z_{17}Z_{18}/(K_{16}(1+Z_{19}/K_{18})+Z_{18})$	$a_{16} = 9.5$	$K_{16} = 1.46105$
u_{17}	$a_{17}Z_{19}/(K_{17}(1+Z_{20}/K_{19})+Z_{19})$	$a_{17} = 0.3$	$K_{17} = 160.0$
u_{18}	$a_{18}Z_{17}Z_{19}/(K_{18}(1+Z_{18}/K_{16})+Z_{19})$	$a_{18} = 16.0$	$K_{18} = 1.46105$
u_{19}	$a_{19}Z_{20}/(K_{19}(1+Z_{19}/K_{17})+Z_{20})$	$a_{19} = 0.27$	$K_{19} = 60.0$

$$P_6(\mathrm{P_S}(t+\Delta t) = '\ \mathrm{A}'|\mathrm{P_S}(t) = '\ \mathrm{Q}') = 1 - \exp\left[-\left(\frac{n_\mathrm{Q}}{1+n_T}\right)\left(\frac{T_\mathrm{Q} - 2T_c}{T_c}\right)\right] \quad (15)$$

We assume that the apoptotic cells stay in the domain for a static time period T_A; later they are vanished due to phagocytosis. We also consider that apoptotic cells gradually lose its mass and radius up to $T_\mathrm{A}/2$ time interval with a fixed rate (Equation (16)). R_0 in Eq. (16) represents the radius of a quiescent cell. After the time duration T_A, apoptotic cells release their occupied positions for the other cells.

$$R_i^{T_\mathrm{A}/2} = R_i^{\left(T_\mathrm{A}/2\right)-\Delta t}\left(1 - \frac{R_0}{T_\mathrm{A}}\right) \quad (16)$$

We consider that a hypoxic cancer cell may alter into necrotic by the influence of the number of neighbouring hypoxic cells (n_H), and the time interval it spends as hypoxic state (T_H). As n_H and T_H increase, the chance of alteration from hypoxic to necrotic is also increased. Hence, P_7 is defined as (Eq. (17))

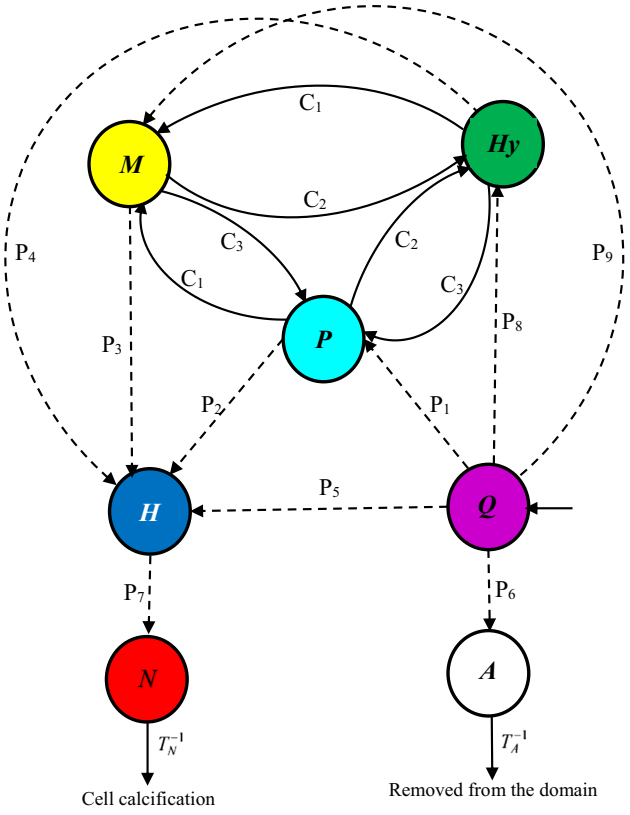

Fig. 3 State-transition diagram for cancer cell phenotype

$$P_7(\mathrm{P_S}(t+\Delta t) = '\ \mathrm{N}'|\mathrm{P_S}(t) = '\ \mathrm{H}') = 1 - \exp\left(-\left(\frac{n_\mathrm{H}}{1+n_T}\right)\left(\frac{T_\mathrm{H} - T_c}{T_c}\right)\right) \quad (17)$$

In Eqs. (15) and (17), n_T and T_C denote the count of cancer cells exist in its neighbouring place and the average cell cycle interval respectively. In this context, we assume that at the time instance t, neighbouring cell(s) of a cell V defines the cancer cell(s) whose centre(s) is within a predefined distance (r) from the centre of V (Fig. 4). Here, $r = 2R_*$.

Necrotic cancer cells degrade as its surface receptors and sub-cellular structure are destroyed. Here, we consider that, initially, the necrotic cell swell up to $\sqrt[3]{2}$ times so that $R_i^t \leq R_*$. After that, it lyse and loose its internal fluids which leads to inactivate the surface receptors. Then calcification initiates [66]. Therefore, cell mass and radius reduce at fixed rates until the radius is 1 μm. We consider that calcification takes T_N time that is divided into T_NL, T_NS, and T_NC which are representing cell swelling, lysing time (T_NL), surface receptors inactivation (T_NS), and calcification time (T_NC), respectively. Therefore, $T_\mathrm{N} = T_\mathrm{NL} + T_\mathrm{NS} + T_\mathrm{NC}$.

Dittmar et al. [19] have recognized that PLCγ is triggered rapidly during cancer cell migration and more slowly during proliferation. PLCγ is also known for

directional movement of cells in the response to the EGF [49]. Therefore, we assume that the rate of change of PLCγ (MM_i in Equation 18) of i^{th} cell decides whether the cell transforms into migratory or not. Researchers Brognard and Dennis, [9, 41, 69] have also experimentally found that, ERK have a strong impact on cell proliferation. Rapid activation of ERK with the EGF leads to cell replication Marshall [46]. Hence, in this study, we assume that the rate of change in ERK (MP_j in Equation 19) of j^{th} cell decides whether a migratory cell proceeds towards proliferative one. Here, we have considered threshold values for PLCγ $\left(X_6^{th}\right)$ and ERK $\left(X_{18}^{th}\right)$ which indicate whether any transformations are taken place in the proliferative cell or migratory cell.

$$MM_i = \left(\frac{dX_6}{dt}\right)_i \tag{18}$$

$$MP_j = \left(\frac{dX_{18}}{dt}\right)_j \tag{19}$$

In this paper, we assume the conditions C_1, C_2, and C_3 which are responsible for transforming the phenotype of a tumour cell among proliferative, migratory, and hybrid cells. The conditions C_1, C_2, and C_3 are the following (Eq. (20)).

$$\left.\begin{aligned} &\mathrm{C}_1 : MP_i > X_6^{th} \text{ and } MM_i < X_{18}^{th} \\ &\mathrm{C}_2 : MP_i > X_6^{th} \text{ and } MM_i > X_{18}^{th} \\ &\mathrm{C}_3 : MP_i < X_6^{th} \text{ and } MM_i > X_{18}^{th} \end{aligned}\right\} \tag{20}$$

A cell i is in quiescent state, may transform into either motile or hybrid state if its parent (Pa(i)) was in motile or in hybrid state and the surrounding microenvironment is suitable. Therefore, the probabilities P_8 and P_9 for the transition from 'Q' to 'M' or 'Q' to 'Hy' are defined as Eqs. (21) and (22), respectively,

$$\begin{aligned} &P_8\left(\mathrm{P_S}(t+\Delta t) =' \mathrm{M}' | \mathrm{P_S}(t) =' \mathrm{Q}' \wedge \mathrm{Pa}(i) =' \mathrm{M}'\right) \\ &= 1 - \exp\left[-\left(\frac{C_\mathrm{N} - \lambda_\mathrm{N}^\mathrm{M}}{\lambda_\mathrm{N}^\mathrm{M}}\right)\left(\frac{C_\mathrm{O} - \lambda_\mathrm{O}^\mathrm{M}}{\lambda_\mathrm{O}^\mathrm{M}}\right)\right] \end{aligned} \tag{21}$$

$$\begin{aligned} &P_9\left(\mathrm{P_S}(t+\Delta t) =' \mathrm{Hy}' | \mathrm{P_S}(t) =' \mathrm{Q}' \wedge \mathrm{Pa}(i) =' \mathrm{Hy}'\right) \\ &= 1 - \exp\left[-\left(\frac{C_\mathrm{N} - \lambda_\mathrm{N}^\mathrm{M}}{\lambda_\mathrm{N}^\mathrm{M}}\right)\left(\frac{C_\mathrm{O} - \lambda_\mathrm{O}^\mathrm{M}}{\lambda_\mathrm{O}^\mathrm{M}}\right)\right] \end{aligned} \tag{22}$$

All the variables in Equations (9) to (22) are dimensionless. The parameters are summarized in Table 4. In Equations (9), (21), and (22), $\lambda_\mathrm{O}^\mathrm{P}$, $\lambda_\mathrm{N}^\mathrm{P}$, $\lambda_\mathrm{O}^\mathrm{M}$, $\lambda_\mathrm{N}^\mathrm{M}$, $\lambda_\mathrm{O}^\mathrm{Hy}$, and $\lambda_\mathrm{N}^\mathrm{Hy}$ are oxygen and nutrient consumptions by the proliferative, motile, and hybrid cells, respectively. For the sake of simplicity, here we consider $\lambda_\mathrm{N}^\mathrm{P} = \lambda_\mathrm{N}^\mathrm{M} = \lambda_\mathrm{N}^\mathrm{Hy}$ and $\lambda_\mathrm{O}^\mathrm{P} = \lambda_\mathrm{O}^\mathrm{M} = \lambda_\mathrm{O}^\mathrm{Hy}$. Similarly in Eq. (13), $\lambda_\mathrm{O}^\mathrm{Q}$ and $\lambda_\mathrm{N}^\mathrm{Q}$ are the consumptions of oxygen and nutrients by the quiescent cells.

3.2 Cancer cell migration

Cell interactions are crucial function for maintaining the tissue structure. In this article, cell-cell and cell-matrix bindings are considered. Here, every cancer cell i is categorized by its radius R_i^t and mass m_i^t at position (x_i, y_i), with its velocity $\left(\overrightarrow{v_i}\right)$ and its state $\mathrm{P_S^i}.(t) R_i^t, m_i^t$, and $\mathrm{P_S^i}(t)$ may change with the cell cycle activities and time. We consider that $\overrightarrow{v_i}$ of a cancer cell in vascular phase varies not only due to the biomechanical forces but also phenotype of a cell. The model considers that five biomechanical forces simultaneously act on the cancer cells: cell-cell adhesion force $\left(\mathbf{F}_{\text{adhesion}}^{i,j}\right)$, cell-cell repulsion force $\left(\mathbf{F}_{\text{repulsion}}^{i,j}\right)$, haptotactic force $\left(\mathbf{F}_{\text{hapto}}^{i}\right)$, chemotactic force $\left(\mathbf{F}_{\text{chemo}}^{i}\right)$, and drag force $\left(\mathbf{F}_{\text{drag}}^{i}\right)$. Hence, total biomechanical forces act on a cancer cell i is

$$\mathbf{F}^i = \underbrace{\mathbf{F}_{\text{drag}}^i}_{\text{drag force}} + \underbrace{\mathbf{F}_{\text{chemo}}^i}_{\text{chemotactic force}} + \underbrace{\mathbf{F}_{\text{hapto}}^i}_{\text{haptotactic force}} + \underbrace{\sum_{\substack{j=1 \\ j\neq i}}^{B(t)} \left(\mathbf{F}_{\text{adhesion}}^{i,j} + \mathbf{F}_{\text{repulsion}}^{i,j}\right)}_{\text{cell - cell interaction force}} \tag{23}$$

In Equation (23), $B(t)$ is the number of cells present in the domain at time t, and $\mathbf{F}^i$ is the collection of applied force on the i^{th} cell. Cell-cell interaction is an important feature in multicellular organism. It helps to maintain an equilibrium in tissue structures. Cancer cells are communicated with each other through the cell surface binding proteins. These binding proteins can bind with the same type as well as other types of receptors of the surrounding cells. Actin polymerization or depolymerisation is a responsible process for changing of morphology of a cancer cell. It helps a cancer cell to extend itself up to a certain distance from its midpoint.

We consider that interaction forces act between the adjacent cancer cells and it affect cell growth, cell division, and cell death mechanisms. It consists of two components: adhesion and repulsion. Adhesion acts between the receptor-ligands on the surface of a cell [45]. The adhesion force

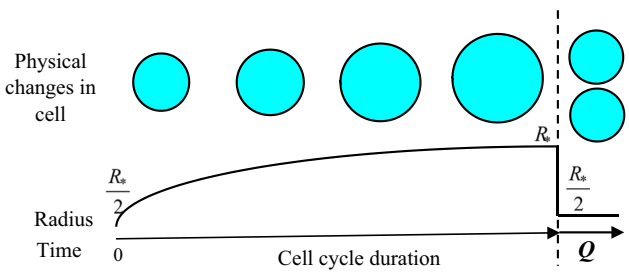

Fig. 4 Life cycle of a tumour proliferative cell

increases with the contact surface area of the adjacent cells. Conversely, cells repel the compression force (by the repulsion force) from the adjacent cells with the help of surface tension of the membranes, cytoskeletons structure, and cytoplasm incompressibility [45]. Both of these forces are weak forces (Fig. 5).

In this paper, we assume that every cancer cells are circular in shape irrespective of the phenotype and it can extend itself beyond its radius to maintain the adhesive binding (except the migratory cells) with the adjacent cells. In this research, it is considered that a cancer cell i with radius R_i^t can maintain the maximum adhesive interaction distance ${}^aR_i^t$ such that ${}^aR_i^t \geq R_i^t$ at time instance t. Here, ${}^aR_i^t = 1.214R_i^t$ [56] at any time instance t. The governing functions (Eqs. (24 and 25)) that represent the adhesion and repulsion forces are as follows:

$$\nabla \mathbf{F}^{i,j}_{\text{adhesion}}\left(\mathbf{d}, {}^aR_i^t\right) = \begin{cases} \left(\frac{1}{2} + \frac{|\mathbf{d}|^3}{2\left({}^aR_i^t\right)^3} - 3\frac{|\mathbf{d}|^2}{2\left({}^aR_i^t\right)^2} + 3\frac{|\mathbf{d}|}{2\left({}^aR_i^t\right)}\right)\frac{\mathbf{d}}{|\mathbf{d}|} & \text{If } 0 \leq |\mathbf{d}| \leq {}^aR_i^t \\ 0 & \text{Otherwise} \end{cases} \tag{24.1}$$

$$\nabla \mathbf{F}^{\mathbf{i,j}}_{\mathbf{repulsion}}\left(\mathbf{d}, {}^aR_i^t\right) = \begin{cases} -\left(\frac{|\mathbf{d}|^3}{{}^aR_i^{t3}} - 3\frac{|\mathbf{d}|^2}{{}^aR_i^{t2}} + 3\frac{|\mathbf{d}|}{{}^aR_i^t}\right)\frac{\mathbf{d}}{|\mathbf{d}|} & \text{If } 0 \leq |\mathbf{d}| \leq {}^aR_i^t \\ 0 & \text{Otherwise} \end{cases} \tag{24.2}$$

where $\mathbf{d}$ represents the distance between centre of two cells. Fig. 6a and b describe that the adhesion and repulsion forces vary with the distance between two adult tumour cells. As the gap between two cells increases, the adhesion force (dimensionless) initially increase, but after that, it gets reduced to zero sharply after ${}^aR_i^t$. However, the repulsive force increases with the distance between two cells and turns to zero at ${}^aR_i^t$. Both the adhesion and repulsion forces are weak.

Haptotactic defines cell movement towards attachment of the ECM (F) via integrins (a group of cell surface receptors). It varies with the density of the ECM. The model assumes that the interactions between the motile cells and the ECM create the haptotactic force which affects the tumour growth dynamics. Hence, the haptotactic force is defined as (Eq. (26))

$$\mathbf{F}^i_{\text{hapto}} = -\eta_1 \nabla F \tag{25}$$

where η_1 is the haptotactic coefficient.

Chemotaxis refers to the movement of cells due to a chemosensory signal. Here, it is considered that nutrient acts as chemosensory molecules. Therefore, chemotaxis is defined as (Eq. (27))

$$\mathbf{F}^i_{\text{chemo}} = -\eta_2 \nabla E \tag{26}$$

where η_2 is the chemo-sensitivity coefficient.

We also consider that a drag force for the luminal fluids acts on the cancer cells in the extracellular space. Therefore, the drag force is described as (Eq. (28))

Table 3 Parameter values to simulate Eqs. (2-8)

Parameter	Values	Unit	Reference
k_{20}	10.0	DC	Alarcón et al. [1]
k_{21}	20.0	DC	Sadhukhan et al. [59]
k_{22}	0.03	DC	Sadhukhan et al. [59]
k_{23}	0.40	DC	Alarcón et al. [1]
k_{24}	1.0	DC	Alarcón et al. [1]
k_{25}	0.25	DC	Alarcón et al. [1]
k_{26}	0.007	DC	Alarcón et al. [1]
k_{27}	0.01	DC	Alarcón et al. [1]
k_{28}	0.01	DC	Alarcón et al. [1]
k_{29}	0.10	DC	Alarcón et al. [1]
k_{30}	0.002	DC	Sadhukhan et al. [59]
k_{31}	0.01	DC	Perfahl et al. [51]
k_{32}	0.25	DC	Sadhukhan et al. [59]
k_{33}	0.1	DC	Sadhukhan et al. [59]
J_3	0.01	DC	Alarcón et al. [1]
J_4	0.01	DC	Alarcón et al. [1]
$K_{Z_{22}}$	0.01	DC	Sadhukhan et al. [59]
$K_{Z_{23}}$	0.01	DC	Alarcón et al. [1]
$K_{Z_{24}}$	0.01	DC	Sadhukhan et al. [59]
R_*	9.953	μm	Alarcón et al. [1]
m_*	1.0	ng	https://bionumbers.hms.harvard.edu/

$$\mathbf{F}^i_{\text{drag}} = -\kappa\left|\vec{v_i}\right| \tag{27}$$

In Eq. (28), $\left|\vec{v_i}\right|$ and κ are the i^{th} cancer cell velocity and a constant coefficient, respectively. Here, we disregard the interstitial fluid flow and gravitational force [56].

As per the Newton's 2nd Law of motion, applied forces on cell i is proportional to the acceleration or velocity change. As per Macklin et al. [45], we make an inertia-less consideration for this model. Therefore, we get Eq. (29):

$$\left|m_i \dot{v}_i\right| = \mathbf{F}^i = \underbrace{\mathbf{F}^i_{\text{drag}}}_{\textbf{drag force}} + \underbrace{\mathbf{F}^i_{\text{chemo}}}_{\text{chemotatic force}} + \underbrace{\mathbf{F}^i_{\text{hapto}}}_{\text{haptotactic force}} + \underbrace{\sum_{\substack{j=1 \\ j\neq i}}^{B(t)} \left(\mathbf{F}^{\text{i,j}}_{\text{adhesion}} + \mathbf{F}^{\text{i,j}}_{\text{repulsion}}\right)}_{\text{cell–cell interaction force}}; \tag{28}$$

as per our consideration, $\left|m_i \dot{v}_i\right| \approx 0$.

Hence, from (28) we get $\left|\vec{v_i}\right|$

$$= \frac{1}{\kappa}\left[\underbrace{\mathbf{F}^i_{\text{chemo}}}_{\text{chemotatic force}} + \underbrace{\mathbf{F}^i_{\text{hapto}}}_{\text{haptotactic force}} + \underbrace{\sum_{\substack{j=1 \\ j\neq i}}^{B(t)} \left(\mathbf{F}^{i,j}_{\text{adhesion}} + \mathbf{F}^{i,j}_{\text{repulsion}}\right)}_{\text{cell–cell interaction force}}\right] \tag{29}$$

The simulation parameters are mentioned in Table 4. Algorithm to determine the resultant force, velocity, and the position of a cell is given in the Appendix. We choose t_{mol} (10^{-6} s) in such a way that $t_{\text{mol}} << t_{\text{cell}}$, where t_{cell} is the time

Table 4 Parameter values for the simulation of cellular and tissue layer

Parameters	Value	Unit	References
$[\mathrm{p27}]^{\mathrm{H}}_{th}$	0.60	DC	Sadhukhan et al. [59]
T_c	23.86	h	(From the simulation)
T_A	8.6	h	Macklin et al. [45], Rocha et al. [56]
T_N	15.0	Days	Macklin et al. (45, Rocha et al. [56]
T_{NL}	6.0	h	Macklin et al. [45], Rocha et al. [56]
T_{NS}	18.0	h	Macklin et al. [45], Rocha et al. [56]
T_{NC}	14.0	Days	Macklin et al. [45], Rocha et al. [56]
$\lambda^{\mathrm{P}}_{\mathrm{O}}$	0.1	h^{-1}	Macklin et al. [45], Rocha et al. [56]
$\lambda^{\mathrm{P}}_{\mathrm{N}}$	0.1	h^{-1}	Sadhukhan et al. [59]
$\lambda^{\mathrm{Q}}_{\mathrm{O}}$	0.08	h^{-1}	Sadhukhan et al. [59]
$\lambda^{\mathrm{Q}}_{\mathrm{N}}$	0.08	h^{-1}	Sadhukhan et al. [59]
$\lambda^{\mathrm{H}}_{\mathrm{O}}$	0.06	h^{-1}	Sadhukhan et al. [59]
$\lambda^{\mathrm{H}}_{\mathrm{N}}$	0.06	h^{-1}	Sadhukhan et al. [59]
$\lambda^{\mathrm{h}}_{\mathrm{O}}$	$0.01\ \lambda^{P}_{C}$	h^{-1}	Macklin et al. [45]
$\lambda^{\mathrm{h}}_{\mathrm{N}}$	$0.01\ \lambda^{P}_{E}$	h^{-1}	
$\lambda^{\mathrm{b}}_{\mathrm{O}}$	$0.01\ \lambda^{P}_{C}$	h^{-1}	Macklin et al. [45]
$\lambda^{\mathrm{b}}_{\mathrm{N}}$	$0.01\ \lambda^{P}_{E}$	h^{-1}	
η_1	25κ	$\mu\mathrm{m\ h}^{-1}$	Rocha et al. [56]
η_2	25κ	$\mu\mathrm{m\ h}^{-1}$	
κ	100	DC	Sadhukhan et al. [59]
X^{th}_6	1×10^{-3}	nMs^{-1}	
X^{th}_{18}	12×10^{-10}	nMs^{-1}	
$D_{C_{\mathrm{O}}}$	1000	$\mu\mathrm{m}^2\ \mathrm{h}^{-1}$	Macklin et al. [45], Rocha et al. [56]
$D_{C_{\mathrm{N}}}$	900	$\mu\mathrm{m}^2\ \mathrm{h}^{-1}$	Sadhukhan et al. [59]
D_S	0.36	$\mu\mathrm{m}^2\ \mathrm{h}^{-1}$	Rocha et al. [56]
D_{M_2}	3.60	$\mu\mathrm{m}^2\ \mathrm{h}^{-1}$	Collier et al. [16]
μ_{M_2}	1.0	DC	
ω	1×10^{-9}	s^{-1}	
θ_1	1.0	DC	Franssen et al. [24]
θ_2	1.0	DC	Franssen et al. [24]
${}^{a}R^{t}_{i}$	$1.214R^{t}_{i}$	μm	Macklin et al. [45], Rocha et al. [56]

step to update the cellular layer that is determined from the cell velocity and it is describe in the Appendix.

4 Extracellular layer modelling

In the extracellular layer, Φ is an open-bounded domain where the tumour is growing with the help of oxygen (C_{O}) and nutrients (C_{N}) and the EGF (S) presents on the ECM (F). Also the motile and hybrid cells secrete membrane-bounded MT1-MMP (M_1) and the diffusible MMP-2 (M_2) which remodel the ECM for expanding the tumour. Let T be the time period for evolving the tumour after the angiogenesis.

In the tissue layer, the species of the microenvironment are modelled with the mass conservation equation. Here, we consider that oxygen, nutrients, EGF, and MMP-2 are soluble factors and spread in the ECM through diffusion. These events are modelled as follows,

$$\frac{\partial C_{\mathrm{O}}}{\partial t} = \nabla.\left(D_{C_{\mathrm{O}}} \nabla C_{\mathrm{O}}\right) - \lambda_{\mathrm{O}} C_{\mathrm{O}} \tag{31}$$

$$\frac{\partial C_{\mathrm{N}}}{\partial t} = \nabla.\left(D_{C_{\mathrm{N}}} \nabla C_{\mathrm{N}}\right) - \lambda_{\mathrm{N}} \mathrm{C}_{\mathrm{N}} \tag{32}$$

$$\frac{\partial S}{\partial t} = \nabla.\left(D_S \nabla S\right) - \lambda_S S \tag{33}$$

In Eqs. (31–33), $D_{C_{\mathrm{O}}}, D_{C_{\mathrm{N}}}$, and D_S are the diffusive constants of oxygen, nutrients, and the EGF. λ_{O}, λ_N, and λ_S are the positive parameters that represent uptake for oxygen, nutrients, and EGF. These variables depend on the cancer cell phenotype.

We assume that the alive cancer cells consume nutrients, oxygen, at the rates of $\lambda_{\mathrm{N}}^{\mathrm{P}}$, $\lambda_{\mathrm{N}}^{\mathrm{Q}}$, $\lambda_{\mathrm{N}}^{\mathrm{H}}$,$\lambda_{\mathrm{N}}^{\mathrm{M}}$, $\lambda_{\mathrm{N}}^{\mathrm{Hy}}$, $\lambda_{\mathrm{O}}^{\mathrm{P}}$, $\lambda_{\mathrm{O}}^{\mathrm{Q}}$, $\lambda_{\mathrm{O}}^{\mathrm{H}}$,$\lambda_{\mathrm{O}}^{\mathrm{M}}$, and $\lambda_{\mathrm{O}}^{\mathrm{Hy}}$, respectively. EGF is consumed only by the proliferative, motile and hybrid cells at the rates of λ_S^{P}, λ_S^{M}, and λ_S^{Hy}. The model also considers that the host cells consume nutrients and oxygen at a rate of $\lambda_{\mathrm{N}}^{\mathrm{h}}$ and $\lambda_{\mathrm{O}}^{\mathrm{h}}$ while in other areas in extracellular space nutrients and oxygen decay at a rate of $\lambda_{\mathrm{N}}^{\mathrm{b}}$ and $\lambda_{\mathrm{O}}^{\mathrm{b}}$.

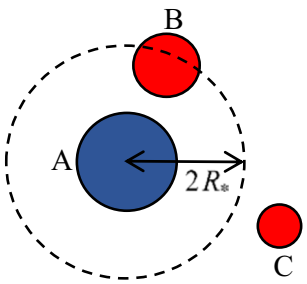

Fig. 5 Cells which present within the fixed radius (r) of cell A are the neighbouring cells of A. According to the rule, B is the neighbouring cell of A but C is not.

We assume that Ω be a small area around a point (x, y) where the cancer cells, host cells, and stroma (non-cells) occupy $\mathrm{f_P}, \mathrm{f_Q}, \mathrm{f_H}, \mathrm{f_M}, \mathrm{f_{Hy}}, \mathrm{f_h}$, and $\mathrm{f_b}$ percent, respectively Hoehme and Drasdo, [35], where $\mathrm{f_P} + \mathrm{f_Q} + \mathrm{f_H} + \mathrm{f_M} + \mathrm{f_{Hy}} + \mathrm{f_h} + \mathrm{f_b} = 1$. Therefore, the consumption rates are described as

$$\lambda_{\mathrm{O}}(x,y) = \mathrm{f_P}\lambda_{\mathrm{O}}^{\mathrm{P}} + \mathrm{f_Q}\lambda_{\mathrm{O}}^{\mathrm{Q}} + \mathrm{f_H}\lambda_{\mathrm{O}}^{\mathrm{H}} + \mathrm{f_M}\lambda_{\mathrm{O}}^{\mathrm{M}} + \mathrm{f_{Hy}}\lambda_{\mathrm{O}}^{\mathrm{Hy}} + \mathrm{f_h}\lambda_{\mathrm{O}}^{\mathrm{h}} + \mathrm{f_b}\lambda_{\mathrm{O}}^{\mathrm{b}} \tag{34}$$

$$\lambda_{\mathrm{N}}(x,y) = \mathrm{f_P}\lambda_{\mathrm{N}}^{\mathrm{P}} + \mathrm{f_Q}\lambda_{\mathrm{N}}^{\mathrm{Q}} + \mathrm{f_H}\lambda_{\mathrm{N}}^{\mathrm{H}} + \mathrm{f_M}\lambda_{\mathrm{N}}^{\mathrm{M}} + \mathrm{f_{Hy}}\lambda_{\mathrm{N}}^{\mathrm{Hy}} + \mathrm{f_h}\lambda_{\mathrm{N}}^{\mathrm{h}} + \mathrm{f_b}\lambda_{\mathrm{N}}^{\mathrm{b}} \tag{35}$$

$$\lambda_S(x,y) = \mathrm{f_P}\lambda_S^{\mathrm{P}} + \mathrm{f_Q}\lambda_S^{\mathrm{Q}} + \mathrm{f_H}\lambda_S^{\mathrm{H}} + \mathrm{f_M}\lambda_S^{\mathrm{M}} + \mathrm{f_{Hy}}\lambda_S^{\mathrm{Hy}} + \mathrm{f_h}\lambda_S^{\mathrm{h}} + \mathrm{f_b}\lambda_S^{\mathrm{b}} \tag{36}$$

Equations (34-36) are demonstrating the uptake rates by the tissue around (x, y). For the sake of simplicity, we consider, in Equations (34-35), $\lambda_{\mathrm{O}}^{\mathrm{P}} = \lambda_{\mathrm{O}}^{\mathrm{M}} = \lambda_{\mathrm{O}}^{\mathrm{Hy}}$ and $\lambda_{\mathrm{N}}^{\mathrm{P}} = \lambda_{\mathrm{N}}^{\mathrm{M}} = \lambda_{\mathrm{N}}^{\mathrm{Hy}}$. In Eq. (36), $\lambda_S^{\mathrm{Q}} = \lambda_S^{\mathrm{H}} = \lambda_S^{\mathrm{h}} = \lambda_S^{\mathrm{b}} = 0$, as EGF is consumed only by the proliferative, motile, and hybrid cells.

The motile and hybrid tumour cells in this model secrete diffusible MMP-2. Hence, MMP-2 describes following Equation (37) with zero flux boundary conditions:

$$\frac{\partial M_2}{\partial t} = \nabla.\left(D_{M_2} \nabla M_2\right) + \mu_{M_2}\left(\mathrm{f_M} + \mathrm{f_{Hy}}\right) - \omega M_2 \tag{37}$$

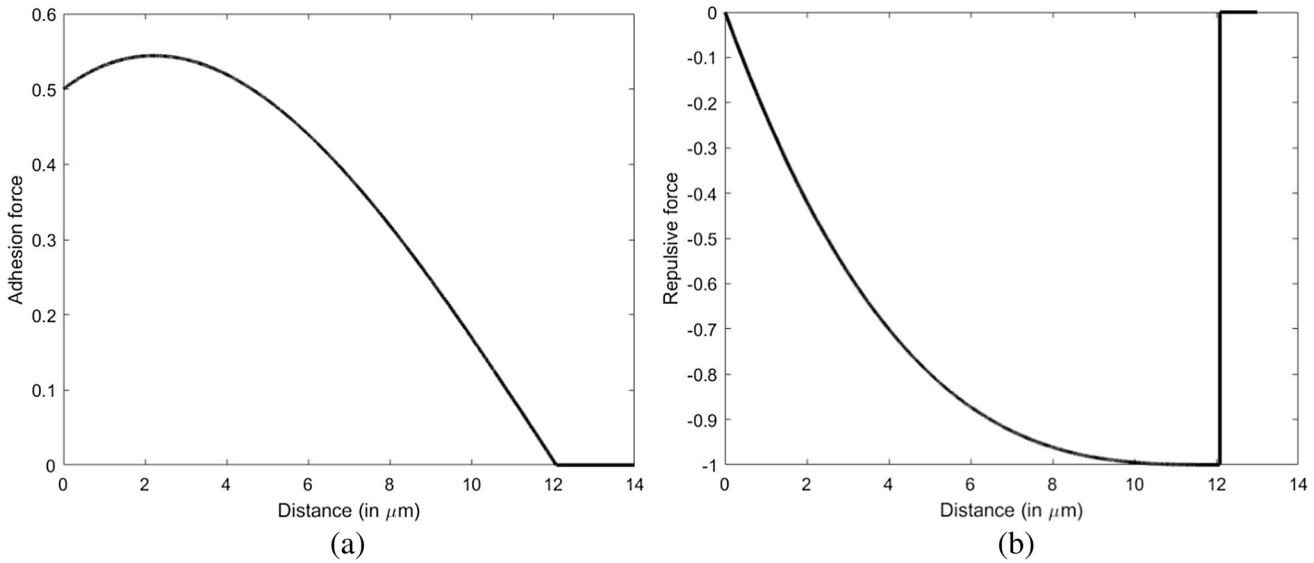

Fig. 6 **a** Adhesion force and **b** repulsive forces for a mature tumour cell.

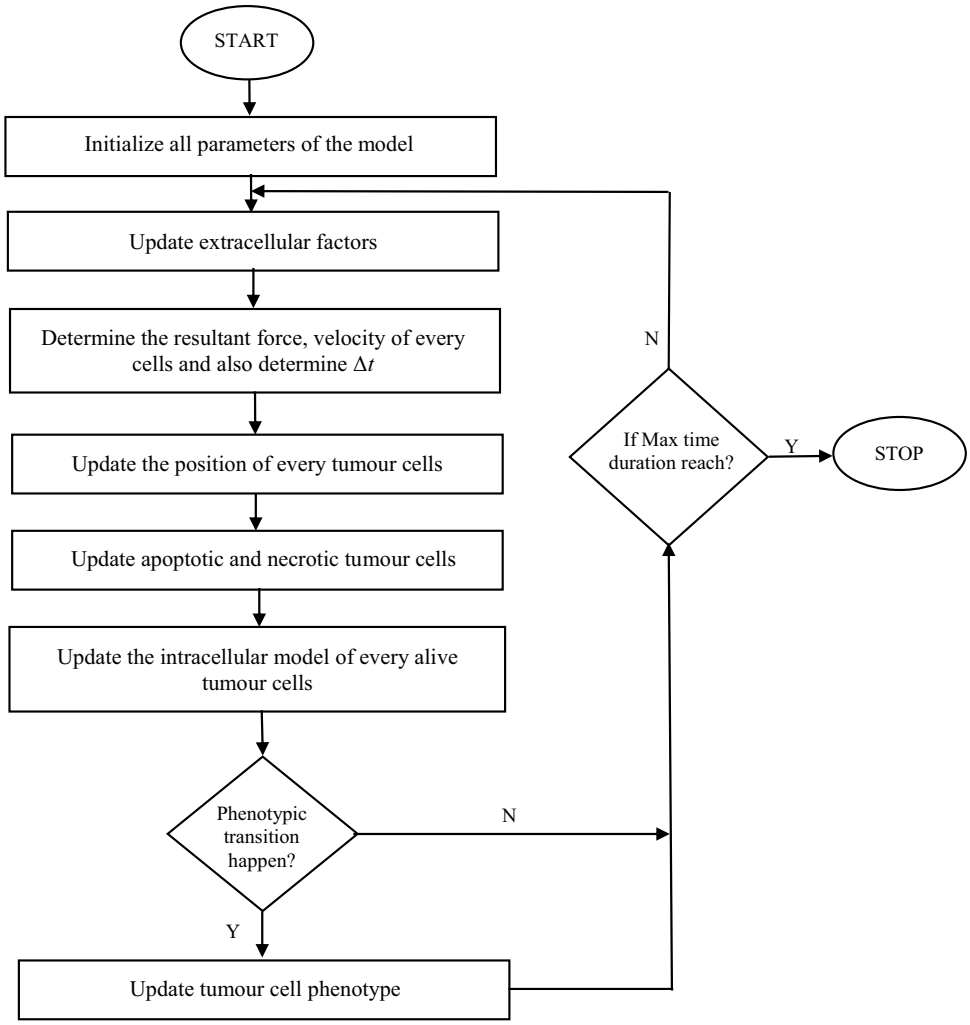

Fig. 7 Flowchart of multi-layered model for cancer cell invasion.

In Eq. (37), D_{M_2} is the diffusion coefficient of MMP-2. μ_{M_2} and ω are the constant terms represented the production by the motile and hybrid tumour cells and the decay rates respectively. Here, $\mu_{M_2}, \omega > 0$. Moreover, motile and hybrid cells express MT1-MMP that bound to the cancer cell membrane and acts locally. Bounded MT1-MMP and diffusible MMP-2 degrade/remodel the ECM with degrading rates θ_1 and θ_2, respectively, $\theta_1, \theta_2 > 0$. The ECM density is governed by Eq. (38) along with zero flux boundary condition:

$$\frac{\partial F}{\partial t} = -\left(\theta_1\left(\mathrm{f_M} + \mathrm{f_{Hy}}\right) + \theta_2 M_2\right)F \tag{38}$$

Cancer cells secrete MMP-2 to remodel the ECM. Therefore, the uptake of this species is interpreted from the cellular scale to tissue scale and vice versa. In this paper, information is exchanged between the two layers (cellular and tissue layer) through two nested grids W_1 and W_2. Step size of these layers are L_1 and L_2, respectively, such that $L_2 = L_1/H$. H is a positive even number. Any point j with position (x_j, y_j) in W_1 is modified with the mean value of the corresponding grid in W_2 which contain the points (x_q, y_q), such that

$$\left|x_q - x_j\right| < L_2\frac{H}{2}, \left|y_q - y_j\right| < L_2\frac{H}{2} \tag{39}$$

5 Simulation and results

Here, a 2-D domain of size [0, 1] mm × [0, 1] mm is taken for the simulation with the other factors. Two grids W_1 and W_2 are considered which exchange information of these factors from one layer to another. W_1 contains 101×101 spatial points, whereas W_2 consists of 1001×1001 points. The step size of W_1 and W_2 are $L_1 = 10$ μm, and $L_2 = 1$ μm, respectively.

The flowchart of this model is described in Fig. 7. Microenvironment of cancer cells are updated after

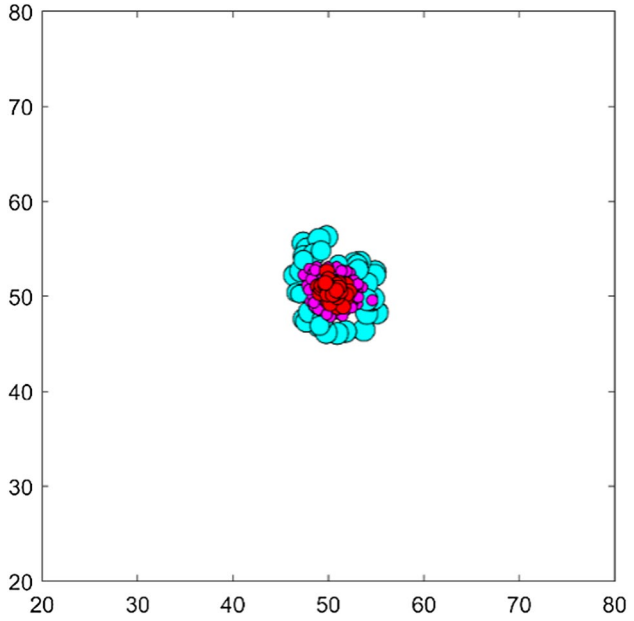

Fig. 8 Cancer cell distribution at $t = 0$. Thirty-seven proliferative cells (cyan coloured), 56 quiescent cells (magenta coloured), 3 hypoxic cells (blue coloured), and 50 necrotic cells (red coloured) are placed in the centre of the domain.

initialization. The resultant physical force on every tumour cells is determined and modified their position and velocity. The mass and radius of the dead tumour cells are also modified concurrently. The subcellular model for the alive cancer cells is executed with the coordination of the external factors. These events modify the state of the alive cancer cells if needed. After that, new values of extracellular species are exchanged to the corresponding grid. These processes are continued until it reaches to the predetermined time period. The code for this algorithm is written in C++, and the visualization part is performed in MATLAB R2017a.

5.1 Execution

To show the ability how much the proposed model can adapt the key characteristics of an invasive cancer, it is executed with the mentioned variables (Tables 1, 2, 3, and 4). The value of these variables are adapted from the previous literatures mostly, but few of them are very difficult to find out. Therefore, these variables are assigned value from the phenomenological arguments. We show the outcomes of the model in different extracellular conditions. We examine the contribution of the ECM and EGF in cancer invasion. Here, four experiments are performed with four different

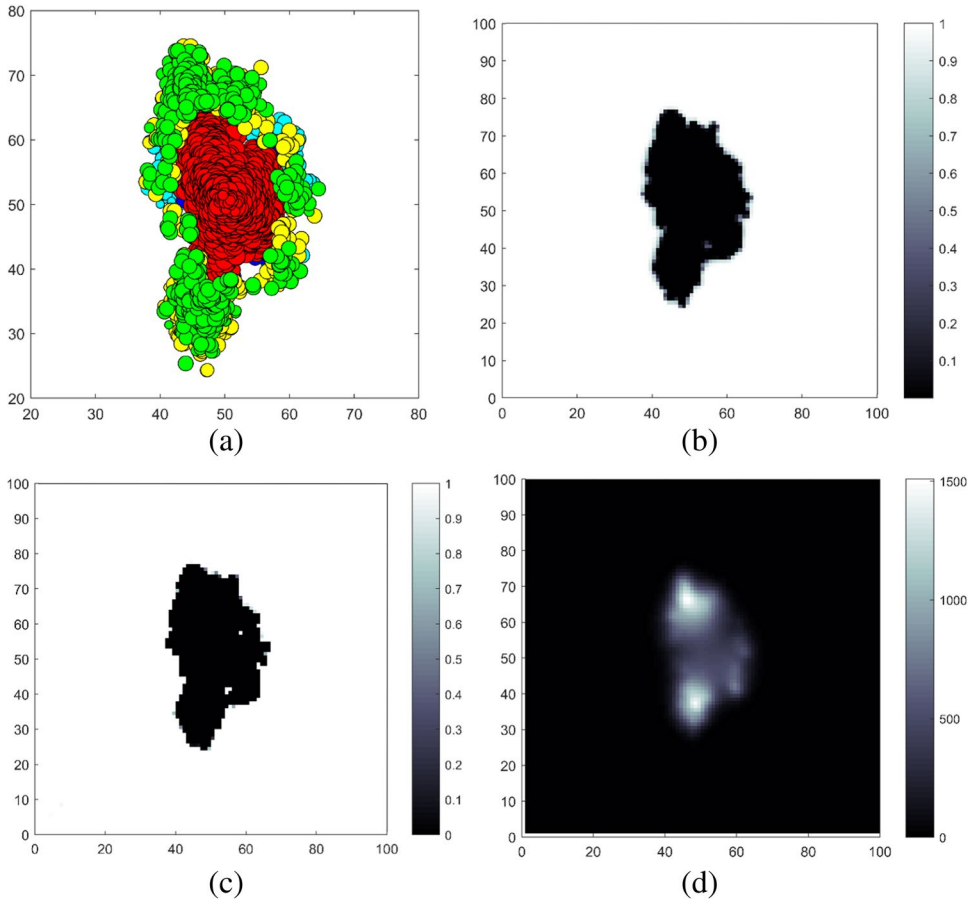

Fig. 9 Simulation result for experiment 1: **a** spatial distributions of invasive tumour cells after 20 simulation days. Necrotic cells (red coloured) and hypoxic cells (blue coloured) are present at the centre, surrounded by the proliferative cells (cyan coloured), migratory cells (yellow coloured), and hybrid cells (green coloured); **b** EGF absorbed by the proliferative, migratory, and hybrid cells; **c** the ECM degradation due to diffused MMP-2 and cell membrane-bounded MT1-MMP by the migratory and hybrid cells; **d** diffused MMP-2 by the migratory and hybrid cells.

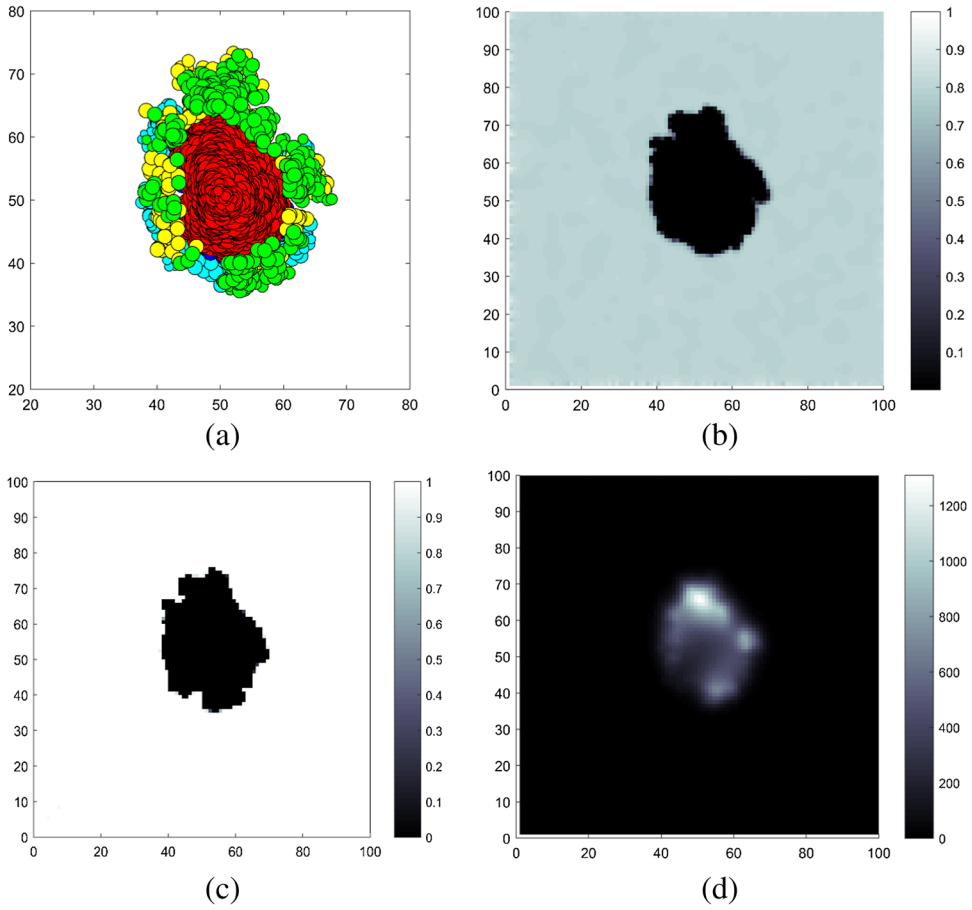

Fig. 10 Simulation result for experiment 2: **a** spatial distributions of invasive tumour cells after 20 simulation days. Necrotic cells (red coloured) and hypoxic cells (blue coloured) are present at the centre, surrounded by the proliferative cells (cyan coloured), migratory cells (yellow coloured), and hybrid cells (green coloured); **b** EGF absorbed by the proliferative, migratory, and hybrid cells; **c** the ECM degradation due to diffused MMP-2 and cell membrane-bounded MT1-MMP by the migratory and hybrid cells; **d** diffused MMP-2 by the migratory and hybrid cells.

distributions of the ECM and EGF. The descriptions are as follows:

Experiment 1: $F[i,j] = 1.0$ and $S[i,j] = 1.0 \forall i,j$ at $t = 0$.
Experiment 2: $F[i,j] = 1.0$ and $0 \leq S[i,j] \leq 1.0 \forall i,j$ at $t = 0$. $S[i,j]$ is generated randomly.
Experiment 3: $0 \leq F[i,j] \leq 1.0$ and $S[i,j] = 1.0 \forall i,j$ at $t = 0$. $F[i,j]$ is generated randomly.
Experiment 4: $0 \leq F[i,j] \leq 1.0$ and $0 \leq S[i,j] \leq 1.0 \forall i,j$ at $t = 0$. $F[i,j]$ and $S[i,j]$ are randomly generated.

We want to develop a model that produce truthful outcomes as well as it helps to explain the fundamental biology of cancer cell invasion. Each experiment is executed thrice, and every time a set of proliferative, quiescent, hypoxic, apoptotic, and necrotic cells are positioned at the centre of the domain initially. In this context, 37 proliferative, 56 quiescent, 3 hypoxic, and 50 necrotic cells are placed in the domain space (Fig. 8). All the experiments are performed in uniformly distributed oxygen and nutrients rich microenvironment. Hence, $C_O[i,j] = C_N[i,j] = 1.0$, and $M_2[i,j] = 0.0 \forall i,j$ at $t = 0$ for all the experiments.

Fig. 9 describes one of the executed outcomes for the experiment 1. The execution starts at $t = 0$ with the initially placed cancer cells (Fig. 8) of the domain. Moreover, the ECM and EGF are uniformly distributed in the domain. The invasive cancer grows by absorbing the surrounding nutrients, oxygen, and EGF. Absorbed EGF (Fig. 9b) activates EGF-EGFR pathway which help the proliferative cells to change their phenotype. At the initial phase, motile and hybrid cells are absent in the domain. From the tumour cell distribution (Fig. 10), it can be observed that the necrotic/dead cells (red coloured) acquired the central region of the tumour. The outer region of the tumour is surrounded by a layer of proliferative cells (cyan coloured) which are the most aggressive among all the phenotypes and continue to proliferate on the boundary. A layer of quiescent cells (magenta coloured) are present in between the necrotic core and the proliferative layer initially. As the simulation goes on, the proliferative cells increase gradually. Necrotic core also increases with the total tumour cells. Some of the proliferative cells are converted into migratory (yellow coloured) and hybrid (green coloured) cells. The migratory and hybrid cells secrete MMP-2 (Fig. 9d) and express MT1-MMP which remodel the homogenously distributed ECM (Fig. 9c). The migratory cells are less proliferative but more motile, whereas hybrid cells are motile as well more proliferative than motile cells. Both of these phenotypes invade

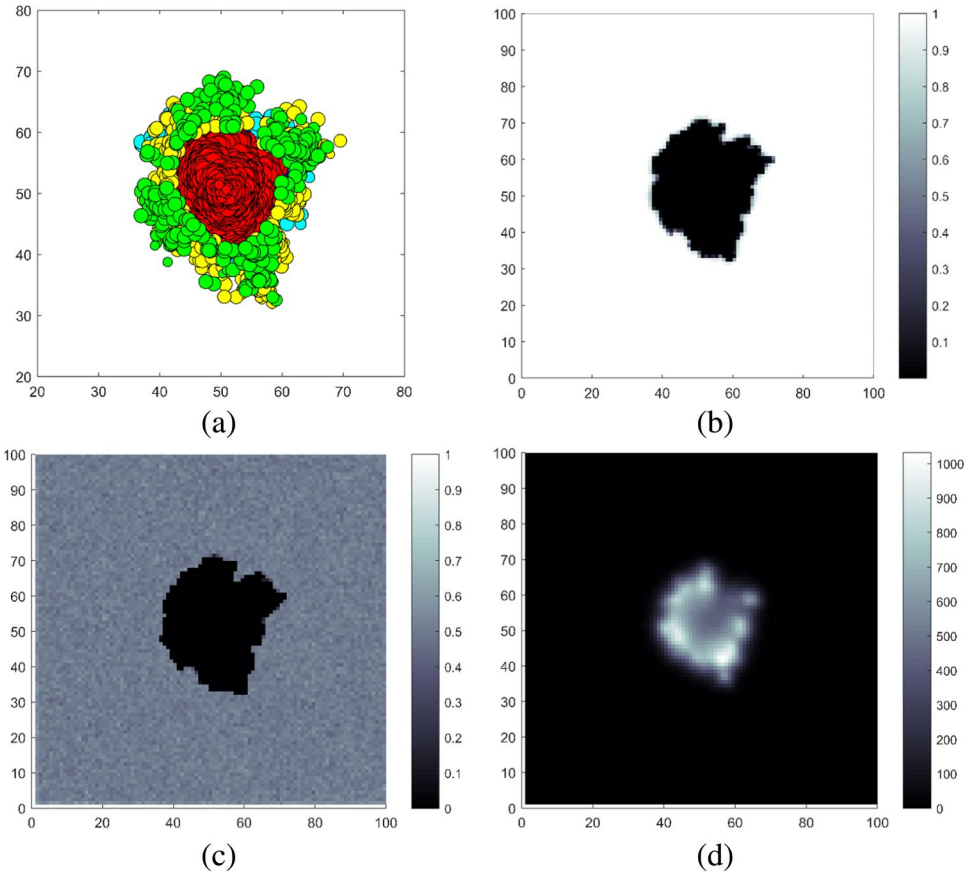

Fig. 11 Simulation result for experiment 3: **a** spatial distributions of invasive tumour cells after 20 simulation days. Necrotic cells (red coloured) and hypoxic cells (blue coloured) are present at the centre, surrounded by the proliferative cells (cyan coloured), migratory cells (yellow coloured), and hybrid cells (green coloured); **b** EGF absorbed by the proliferative, migratory, and hybrid cells; **c** the ECM degradation due to diffused MMP-2 and cell membrane-bounded MT1-MMP by the migratory and hybrid cells; **d** diffused MMP-2 by the migratory and hybrid cells.

the surrounding tissue (ECM) through the less resistant path (Fig. 9a).

Fig. 10a–d illustrates one of the simulated outcomes for the experiment 2 with random EGF distribution. The tumour cell distributions are radically different showing more finger-like morphology. Like the previous experiment 1, here four types of tumour cells are observed (Fig. 10a). Necrotic core is seen at the centre of tumour. Necrotic core is surrounded by proliferative cells, migratory cells, and hybrid cells. As EGF is randomly distributed (Fig. 10b) in the domain space, less number of migratory and hybrid cells are produced than the previous experiment. Migratory and hybrid cells secrete MMP-2 (Fig. 10d) and MT1-MMP which remodel the ECM (Fig. 10c). The migratory and hybrid cells mainly develop finger-like protrusions which move through the less resistance path.

Fig. 11a–d provides one of the simulation results for the experiment 3 with randomly distributed ECM. Here also four types of tumour cell are seen (Fig. 11a). Necrotic core is observed at the centre of tumour. The necrotic core is surrounded by proliferative, migratory, and hybrid cells respectively. Less number of proliferative cell load are observed at the end of 20 simulation days. The ECM is randomly distributed (Fig. 11b) in the domain space. The tumour cell distributions are showing less finger-like morphology like the previous one (experiment 2). Secretion of MMP-2 (Fig. 11d) and MT1-MMP by the migratory and hybrid cells remodel the ECM (Fig. 11c). The migratory and hybrid cells mainly develop finger-like protrusions.

Fig. 12a–d describe one of the outcomes for the experiment 4 with randomly distributed EGF and the ECM. Here five types of tumour cell are observed (Fig. 12a). Necrotic core is visible at the centre of tumour. It is surrounded by a few hypoxic cells. Proliferative, migratory, and hybrid cells are present at the outer layer of the tumour. As EGF and the ECM are randomly distributed (Fig. 12(b-c)) in the domain space showing less finger-like morphology in the tumour. Migratory and hybrid cells secrete MMP-2 (Fig. 12d) and MT1-MMP which remodels the ECM (Fig. 12c).

We have also plotted the avg. number of proliferative, migratory, and hybrid cells for these four experiments (Fig. 13a–d). All of these figures show same kind of patterns for these three phenotypes. Initially, the proliferative cells increase by absorbing oxygen and nutrients which are available in the domain in sufficient level. But after a certain period (~7 simulation days), it reduces sharply. Nearly 10 simulation days, its reduction rate is decreased, and it continues until 20 simulation days. On the other hand, migratory and hybrid cells are absent in the domain initially. With the help of EGF, some of the proliferative cells converted into

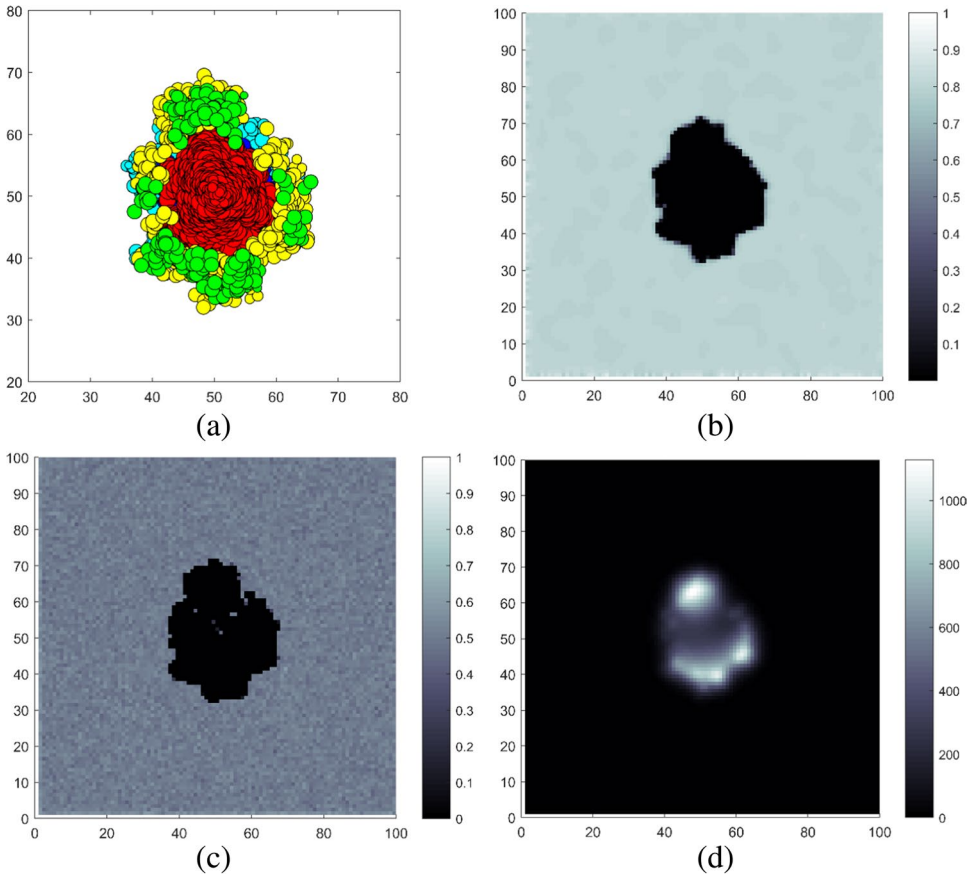

Fig. 12 Simulation result for experiment 4: **a** spatial distributions of invasive tumour cells after 20 simulation days. Necrotic cells (red coloured) and hypoxic cells (blue coloured) are present at the centre, surrounded by the proliferative cells (cyan coloured), migratory cells (yellow coloured), and hybrid cells (green coloured); **b** EGF absorbed by the proliferative, migratory, and hybrid cells; **c** the ECM degradation due to diffused MMP-2 and cell membrane-bounded MT1-MMP by the migratory and hybrid cells; **d** diffused MMP-2 by the migratory and hybrid cells.

migratory or hybrid phenotypes. These two phenotypes are gradually increases in the tumour, and after a certain time, the number of migratory and hybrid cells would be much more than the proliferative cells (except in experiment 2). The migratory and hybrid cells are mainly responsible for tumour invasion which may lead to metastasis. These graphical representations are very similar to the trends that were reported by Zhang et al. [75], Wang et al. [70], and Chen et al. [14].

Further, we plot the avg. proliferative (Fig. 14), migratory (Fig. 15), and hybrid (Fig. 16) cells for all the conditions (experiments 1, 2, 3, and 4). It is observed from Fig. 14 that, for experiments 1 and 3 and experiments 2 and 4, same kinds of patterns are found for avg. tumour cell counts. It indicates that the ECM density distribution does not effect on the proliferative cell count. However, in Fig. 15, it is shown that experiments 1 and 3 produce same kind of pattern, whereas experiment 4 produces an upper bound and experiment 2 seems to be a lower bound for avg. migratory cell counts. This indicates that, though the EGF density distributions is mainly responsible for the production of migratory cells, the ECM density distributions also effect on the avg. count of migratory cells. In experiment 4, where ECM density lies between 0 and 1, MDEs (MT1-MMP and MMP-2) play a major role to remodel the ECM. These phenomena produce lot of spaces for more number of migratory cells. On the other hand, in experiment 2, the ECM is denser than experiment 4. So, creating space with the MDEs are time-consuming tasks. Hence, the avg. number of migratory cells are very low among all the experiments. Fig. 16 shows different types of pattern for avg. hybrid cell counts. Here, experiments 2 and 3 show same kind of patterns, whereas experiment 1 seems to be an upper bound and experiment 4 produces a lower bound. It indicates that denser ECM and EGF produce more number of hybrid cells. In the experiments 2, 3, and 4, one or both of the factors between EGF and the ECM are less dense which effect avg. hybrid cell counts.

6 Discussions and conclusions

Cancer is a group of diseases involving abnormal cell growth with the potential to invade or spread to other parts of the body. To defeat cancer, it is very important to understand cancer formation, progression, and control. But still most of the processes involved in tumour growth are not clearly understood. Mathematical models can enhance this understanding of this dynamical process and underpinning cancer invasion and metastatic spread. Mathematical models can

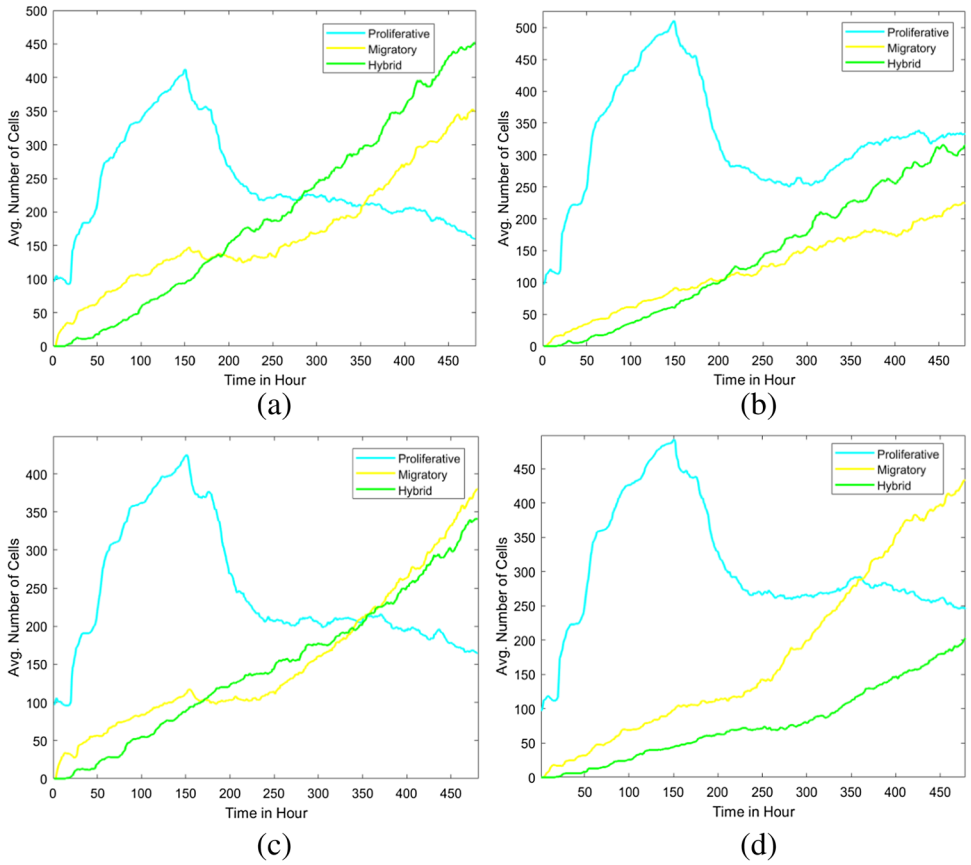

Fig. 13 Avg. cell counts of proliferative, migratory, and hybrid cells in **a** experiment 1, **b** experiment 2, **c** experiment 3, and **d** experiment 4, respectively.

get rid of this situation through real-time observation of cellular distribution, cell movements, genetic mutations, etc.

In general, oncologists are treating a patient by examining and classifying cancer type that decides the treatment plan. Oncologists follow the same treatment path that has worked for the patients with similar symptoms and disease state in the past, though this idea is not fruitful for all but a subset of patients. In most cases, the same treatment plan either does not work or results even more adverse. The reason behind this partial success is due to own genetic makeup of every tumour that implies a unique response to

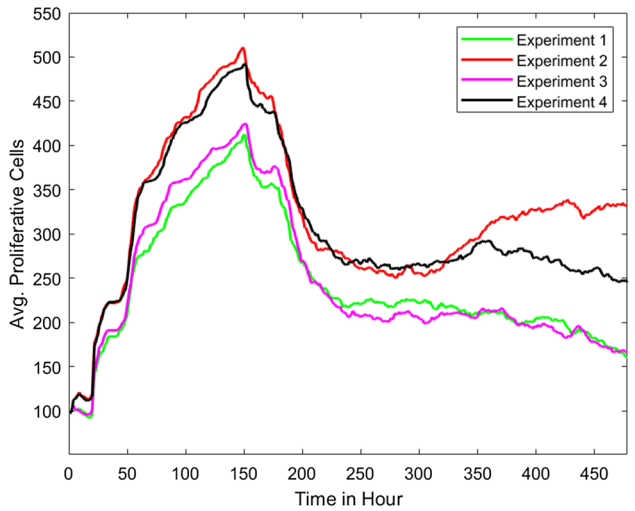

Fig. 14 Avg. proliferative cell counts in experiments 1, 2, 3, and 4, respectively.

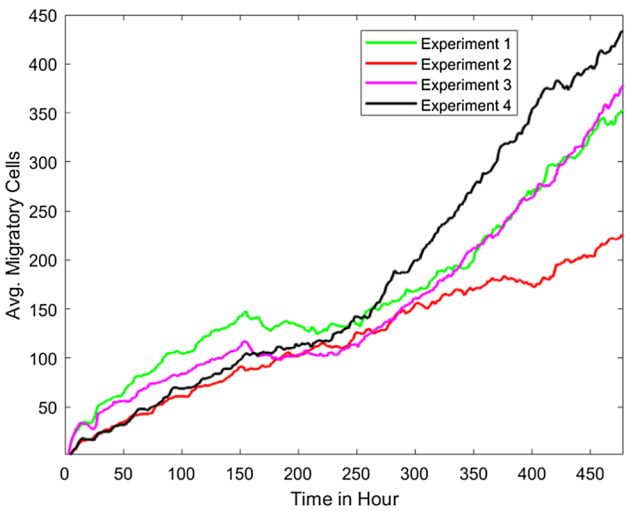

Fig. 15 Avg. migratory cell counts in experiments 1, 2, 3, and 4, respectively.

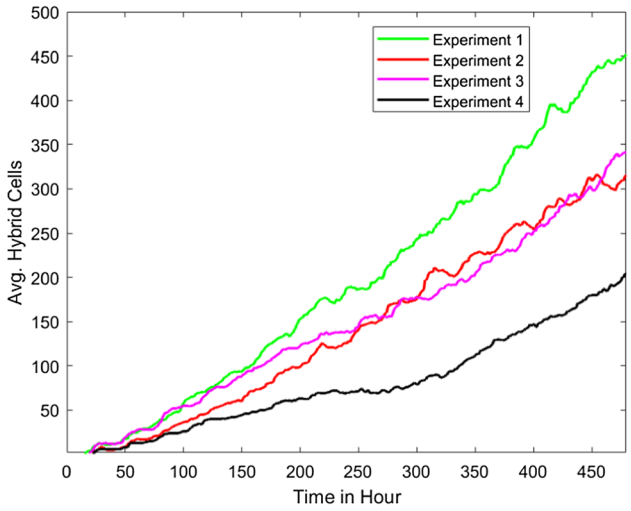

Fig. 16 Avg. hybrid cell counts in experiments 1, 2, 3, and 4, respectively.

the treatment applied. Our model can be further enhanced for advanced cancer treatment where modern diagnostic techniques together with the model could be used in clinical setting with large amounts of data on patients' outcome. Accurate models allow us to treat patients theoretically in non-invasive way within a short span of time [17]. Simulation outcomes of individually parameterized relevant mathematical models for a particular patient helps the oncologists to choose the best possible treatment plan, their best timing, and the optimal dosage [55] to be used. Integration of these models with proper biomarkers and imaging data could be useful in precision medicine or patient-specific treatment. These models would not only be capable enough to forecast the tumour evolution but also provide the optimal treatment procedure for a specific patient. Although it is very difficult to find out actual patient data in the vascular phase, the model could help to predict the invasion accurately. Further, the model could be extended to predict the affected organs during metastasis at an early stage.

In this article, a multi-layered hybrid model is developed for cancer invasion in a 2-D framework. The model assumes that each cancer cell is a cellular agent. These cellular agents can have different characteristics: some are more proliferative but less motile, some are more motile and less proliferative, and some are the combination of these two. Also hypoxic, necrotic, quiescent, and apoptotic cellular agents are considered in the domain space. A cellular agent can be transformed into any of the phenotype depending upon its internal proteins expression and its surrounding microenvironment. These agents communicate with each other and the surroundings through cell-cell interactions, cell-matrix interactions, etc.; these interactions create several physical forces that act concurrently on the cancer cells (agents) and help them to migrate in the extracellular space. The model also considers that membrane-bounded MT1-MMP and the diffusible MMP-2 secreted by the motile and hybrid cells are the main actors for the ECM degradation.

There are multiple validation techniques available like mathematical, statistical, and graphical methods to perform sensitivity analysis of mathematical models. These methods are different one over the another in terms of applicability, computational issues, complexity, and representations. To validate this model, we have performed sensitivity analysis Basu and Roy [6]. Sensitivity analysis is mainly used to study the robustness of the model by varying one or more than one input variables. If the outcome of the model varies drastically with the values of input parameters, then the conclusion has been drawn that the model is extensively sensitive to the parameters and it requires further refinement [22, 39, 67], Jenerette and Wu [36].

In this case, we have performed a partial sensitivity analysis (Table 5) by determining the effect of the outcome by changing some of the input variables while keeping other parameters fixed. The sensitivity of the model is performed through the root mean square deviation (RMSD) percentage with respect to the outcomes of experiment 1. The analysis is performed couple of times by varying the values of λ_O, λ_N, λ_S, μ_{M_2}, ω, Θ_1, and Θ_2 by $\pm 5\%$, $\pm 10\%$ and keeping other parameter fixed (in Experiment 1).

Table 5 Measuring RMSD for different cell counts after 480h of simulation time by changing λ_O, λ_N, λ_S, μ_{M_2}, ω, Θ_1, and Θ_2

Cell counts	+10%	+5%	Without changing parameters	−5%	−10%	RMSD	RMSD (in %)
No. of more proliferative cells	63	98	160	64	62	89.54	55.96
No. of more motile cells	318	367	350	455	492	90.14	25.75
No. of hybrid cells	402	391	452	619	581	112.63	24.92
No. of necrotic cells	937	894	1050	1171	1192	113.58	10.81
No. of total cells	1795	1826	2133	2381	2438	301.25	14.12

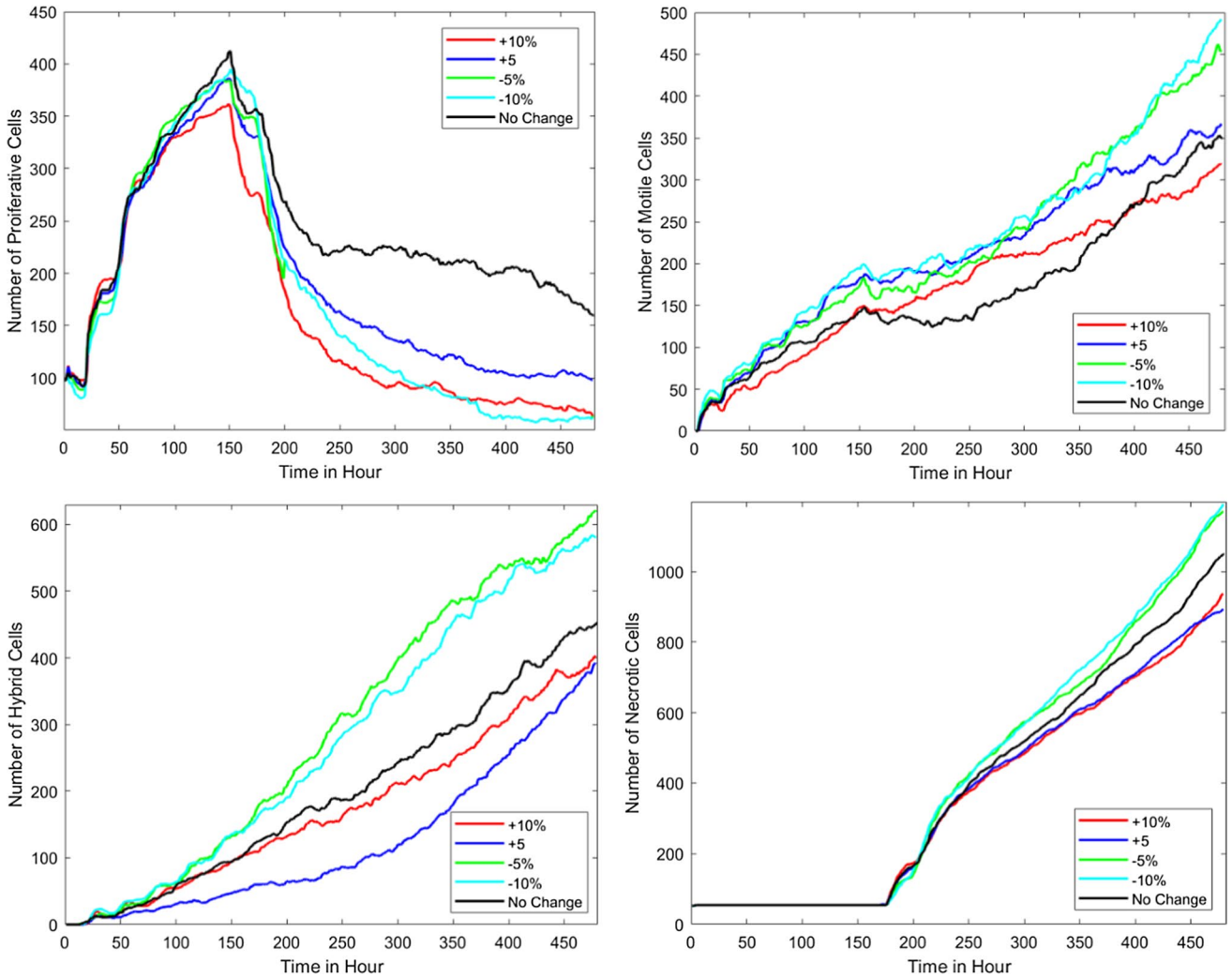

Fig. 17 Number of proliferative (upper-left), motile (upper-right), hybrid (lower-left), and necrotic (lower-right) cells for experiment 1 by changing the respective variables by +10%, +5%, −5%, and −10% and without changing the variables.

In this case, the RMSD percentage for number of proliferative cell is moderately high (55.96), although the other RMSD percentages like number of motile cells, number of hybrid cells, number of necrotic cells, and total number of tumour cells are 25.75, 24.92, 10.81, and 14.12, respectively. The RMSD percentages indicate that the number of proliferative cell is moderately sensitive to the specified parameters' values, while the other ones are less sensitive to these parameters (Fig. 17).

The aim of the paper is to study the tumour cell heterogeneity due to the geometrical changes of a growing tumour caused by the mutations of cells. In this context, four different experiments are conducted with four different configurations of the ECM and EGF. Every time the geometrical changes are observed and are correlated with the proliferative, migratory, and hybrid cell count. Also the effect of the ECM and EGF on proliferative, migratory, and hybrid cell counts has been studied. The outcome of the model is very similar to the reported results in earlier studies [70, 75],and [14]. Hanahan and Weinberg [29] have investigated the complexity within cancer by acquiring the common features of several cancer cells that indicate influential hallmarks of cancer. Our model also covers the important characteristics of cancer invasion mentioned in Hanahan and Weinberg [29].

Appendix

Algorithm for determining the net acting force, velocity, and the position of a cell:

Step 1: While $t \le t_{\text{tissue}}$ //Here, we consider $t_{\text{tissue}} = 60$ min

For $i = 1$ to $B(t)$

For $j = 1$ to $B(t)$

Step 2: if $i == j$

Continue;

End if

Step 3: $\mathbf{F}^i = \mathbf{F}^i + \left(\mathbf{F}^{i,j}_{\text{adhesion}} + \mathbf{F}^{i,j}_{\text{repulsion}}\right)$

End For

Step 4: $\mathbf{F}^i = \mathbf{F}^i + \left(\underbrace{\mathbf{F}^i_{\text{drag}}}_{\text{drag force}} + \underbrace{\mathbf{F}^i_{\text{chemo}}}_{\text{chemotactic force}} + \underbrace{\mathbf{F}^i_{\text{hapto}}}_{\text{haptotactic force}} \right)$

Step 5: End For

Step 6: For = 1 to $B(t)$

$\mathbf{v}_i \leftarrow \mathbf{F}^i$

End For

Step 7: $t_{\text{cell}} \leftarrow \dfrac{1}{\mathbf{max}\left(\left\|\mathbf{v}_i\right\|\right)}$ //Time step t_{cell} is determined for updating cellular layer

Step 8: For = 1 to $B(t)$

$\mathbf{X}_i \leftarrow \mathbf{X}_i + \left|\mathbf{v}_i\right|.t_{\text{cell}}$ //New position of cell i is defined

End For

Step 9: $t \leftarrow t + t_{\text{cell}}$

Step 10: End While

Acknowledgements We would like to thank Dr. Nitish Thakor, Editor-in-Chief, *Medical & Biological Engineering & Computing Journal* for being supportive towards the publication of this paper. We show our sincere gratitude to the anonymous reviewers, whose valuable comments helped us greatly to improve this article. We are also thankful to Dr. S. K. Basu for his contribution in this article. The first author of this paper is thankful to the University Grant Commission, Government of India for supporting him with a Senior Research Fellowship.

Declarations

Conflict of interest The authors declare no competing interests.

References

1. Alarcón T, Byrne HM, Maini PK (2004) A mathematical model of the effects of hypoxia on the cell-cycle of normal and cancer cells. J Theor Biol 229(3):395–411
2. Ambrosi D, Preziosi L (2002) On the closure of mass balance models for tumor growth. Mathe Mod Methods Appl Sci 12(05):737–754
3. Andasari V, Gerisch A, Lolas G, South AP, Chaplain MA (2011) Mathematical modeling of cancer cell invasion of tissue: biological insight from mathematical analysis and computational simulation. J Mathe Biol 63(1):141–171

4. Anderson AR, Chaplain MA, Newman EL, Steele RJ, Thompson AM (2000) Mathematical modelling of tumour invasion and metastasis. Comput Mathe Methods Med 2(2):129–154
5. Athale C, Mansury Y, Deisboeck TS (2005) Simulating the impact of a molecular 'decision-process' on cellular phenotype and multicellular patterns in brain tumors. J Theor Biol 233(4):469–481
6. Basu SK, Roy A (2004) Computer simulation of long-term vegetation status in landslide-prone areas in the Himalayan region. Simulation 80(10):511–525
7. Bonnans C, Chou J, Werb Z (2014) Remodelling the extracellular matrix in development and disease. Nat Rev Mol Cell Biol 15(12):786–801
8. Brightman FA, Fell DA (2000) Differential feedback regulation of the MAPK cascade underlies the quantitative differences in EGF and NGF signalling in PC12 cells. FEBS Lett 482(3):169–174
9. Brognard J, Dennis PA (2002) Variable apoptotic response of NSCLC cells to inhibition of the MEK/ERK pathway by small molecules or dominant negative mutants. Cell Death Differ 9(9):893–904
10. Carmeliet P, Jain RK (2000) Angiogenesis in cancer and other diseases. Nature 407(6801):249–257
11. Chaplain MA, Lolas G (2005) Mathematical modelling of cancer cell invasion of tissue: The role of the urokinase plasminogen activation system. Mathe Mod Methods Appl Sci 15(11):1685–1734
12. Chaplain MA, Lolas G (2006) Mathematical modelling of cancer invasion of tissue: dynamic heterogeneity. Netw Heterog Media 1(3):399
13. Chaplain MA, Lachowicz M, Szymanska Z, Wrzosek D (2011) Mathematical modelling of cancer invasion: the importance of cell–cell adhesion and cell–matrix adhesion. Mathe Mod Methods Appl Sci 21(04):719–743
14. Chen Y, Wang H, Zhang J, Chen K, Li Y (2015) Simulation of avascular tumor growth by agent-based game model involving phenotype-phenotype interactions. Sci Rep 5(1):1–10
15. Chicoine MR, Silbergeld DL (1997) Mitogens as motogens. J Neuro-Oncol 35(3):249–257
16. Collier IE, Legant W, Marmer B, Lubman O, Saffarian S, Wakatsuki T, … Goldberg GI (2011) Diffusion of MMPs on the surface of collagen fibrils: the mobile cell surface–collagen substratum interface. PLoS One 6(9):e24029
17. Cook LM, Araujo A, Pow-Sang JM, Budzevich MM, Basanta D, Lynch CC (2016) Predictive computational modeling to define effective treatment strategies for bone metastatic prostate cancer. Sci Rep 6(1):1–12
18. Deakin N, Chaplain MA (2013) Mathematical modeling of cancer invasion: the role of membrane-bound matrix metalloproteinases. Front Oncol 3:70
19. Dittmar T, Husemann A, Schewe Y, Nofer JR, Niggemann B, Zänker KS, Brandt BH (2002) Induction of cancer cell migration by epidermal growth factor is initiated by specific phosphorylation of tyrosine 1248 of c-erbB-2 receptor via epidermal growth factor receptor. FASEB J 16(13):1–21
20. Domschke P, Trucu D, Gerisch A, Chaplain MA (2014) Mathematical modelling of cancer invasion: implications of cell adhesion variability for tumour infiltrative growth patterns. J Theor Biol 361:41–60
21. Dongre A, Weinberg RA (2019) New insights into the mechanisms of epithelial–mesenchymal transition and implications for cancer. Nat Rev Mol Cell Biol 20(2):69–84
22. Ehrlén J, Van Groenendael J, De Kroon H (2001) Reliability of elasticity analysis: reply to Mills et al. Conserv Biol 15(1):278–280
23. Franssen LC, Chaplain MA (2020) A mathematical multi-organ model for bidirectional epithelial–mesenchymal transitions in the metastatic spread of cancer. IMA J Appl Mathe 85(5):724–761
24. Franssen LC, Lorenzi T, Burgess AE, Chaplain MA (2019) A mathematical framework for modelling the metastatic spread of cancer. Bull Mathe Biol 81(6):1965–2010
25. Friedl P, Wolf K (2010) Plasticity of cell migration: a multiscale tuning model. J Cell Biol 188(1):11–19
26. Gardner LB, Li Q, Park MS, Flanagan WM, Semenza GL, Dang CV (2001) Hypoxia inhibits G1/S transition through regulation of p27 expression. J Biol Chem 276(11):7919–7926
27. Gerisch A, Chaplain MA (2008) Mathematical modelling of cancer cell invasion of tissue: local and non-local models and the effect of adhesion. J Theor Biol 250(4):684–704
28. Hackel PO, Zwick E, Prenzel N, Ullrich A (1999) Epidermal growth factor receptors: critical mediators of multiple receptor pathways. Curr Opin Cell Biol 11(2):184–189
29. Hanahan D, Weinberg RA (2000) The hallmarks of cancer. Cell 100(1):57–70
30. Handler J, Cullis J, Avanzi A, Vucic EA, Bar-Sagi D (2018) Preneoplastic pancreas cells enter a partially mesenchymal state following transient TGF-β exposure. Oncogene 37(31):4334–4342
31. Hatakeyama M, Kimura S, Naka T, Kawasaki T, Yumoto N, Ichikawa M, … Yokoyama S (2003) A computational model on the modulation of mitogen-activated protein kinase (MAPK) and Akt pathways in heregulin-induced ErbB signalling. Biochem J 373(2):451–46
32. Hendriks BS, Griffiths GJ, Benson R, Kenyon D, Lazzara M, Swinton J, … De Graaf D (2006) Decreased internalisation of erbB1 mutants in lung cancer is linked with a mechanism conferring sensitivity to gefitinib. IEE Proc-Syst Biol 153(6):457–466
33. Hillen F, Griffioen AW (2007) Tumour vascularization: sprouting angiogenesis and beyond. Cancer Metastasis Rev 26(3–4):489–502
34. Hirsch FR, Varella-Garcia M, Bunn Jr PA, Di Maria MV, Veve R, Bremnes RM, … Franklin WA (2003) Epidermal growth factor receptor in non–small-cell lung carcinomas: correlation between gene copy number and protein expression and impact on prognosis. J Clin Oncol 21(20):3798–3807
35. Hoehme S, Drasdo D (2010) Biomechanical and nutrient controls in the growth of mammalian Cell populations. Mathe Popul Stud 17(3):166–187
36. Jenerette GD, Wu J (2001) Analysis and simulation of land-use change in the central Arizona-Phoenix region, USA. Landsc Ecol 16(7):611–626
37. Kawamata H, Nakashiro KI, Uchida D, Harada K, Yoshida H, Sato M (1997) Possible contribution of active MMP2 to lymph-node metastasis and secreted cathepsin L to bone invasion of newly established human oral-squamous-cancer cell lines. Int J Cancer 70(1):120–127
38. Kholodenko BN, Demin OV, Moehren G, Hoek JB (1999) Quantification of short term signaling by the epidermal growth factor receptor. J Biol Chem 274(42):30169–30181
39. Law AM, Kelton WD, Kelton WD (2000) Simulation modelling and analysis, vol 3. McGraw-Hill, New York
40. Lehembre F, Yilmaz M, Wicki A, Schomber T, Strittmatter K, Ziegler D, Kren A, Went P, Derksen PW, Berns A, Jonkers J, Christofori G (2008) NCAM-induced focal adhesion assembly: a functional switch upon loss of E-cadherin. EMBO J 27(19):2603–2615
41. Li M, Lee TW, Yim AP, Mok TS, Chen GG (2006) Apoptosis induced by troglitazone is both peroxisome proliferator-activated receptor-γ-and ERK-dependent in human non-small lung cancer cells. J Cell Physiol 209(2):428–438
42. Liotta LA (1992) Cancer cell invasion and metastasis. Sci Am 266(2):54–63

43. Lovisa S, LeBleu VS, Tampe B, Sugimoto H, Vadnagara K, Carstens JL, … Nischal H (2015) Epithelial-to-mesenchymal transition induces cell cycle arrest and parenchymal damage in renal fibrosis. Nat Med 21(9):998–1009
44. Lozano E, Betson M, Braga VM (2003) Tumour progression: small GTPases and loss of cell–cell adhesion. Bioessays 25(5):452–463
45. Macklin P, Edgerton ME, Thompson AM, Cristini V (2012) Patient-calibrated agent-based modelling of ductal carcinoma in situ (DCIS): from microscopic measurements to macroscopic predictions of clinical progression. J Theor Biol 301:122–140
46. Marshall CJ (1995) Specificity of receptor tyrosine kinase signaling: transient versus sustained extracellular signal-regulated kinase activation. Cell 80(2):179–185
47. Masuda H, Zhang D, Bartholomeusz C, Doihara H, Hortobagyi GN, Ueno NT (2012) Role of epidermal growth factor receptor in breast cancer. Breast Cancer Res Treat 136(2):331–345
48. Montell DJ (2008) Morphogenetic cell movements: diversity from modular mechanical properties. Science 322(5907):1502–1505
49. Mouneimne G, Soon L, DesMarais V, Sidani M, Song X, Yip SC, … Condeelis J (2004) Phospholipase C and cofilin are required for carcinoma cell directionality in response to EGF stimulation. J Cell Biol 166(5):697–708
50. Pastushenko I, Blanpain C (2019) EMT transition states during tumor progression and metastasis. Trends Cell Biol 29(3):212–226
51. Perfahl H, Byrne HM, Chen T, Estrella V, Alarcón T, Lapin A, Gateny RA, Gillies RJ, Lloyd MC, Maini PK, Reuss M, Owen MR (2011) Multiscale modelling of vascular tumour growth in 3D: the roles of domain size and boundary conditions. PloS One 6(4):e14790
52. Price JT, Wilson HM, Haites NE (1996) Epidermal growth factor (EGF) increases the in vitro invasion, motility and adhesion interactions of the primary renal carcinoma cell line, A704. Eur J Cancer 32(11):1977–1982
53. Putnam EA, Yen N, Gallick GE, Steck PA, Fang K, Akpakip B, Roth JA (1992) Autocrine growth stimulation by transforming growth factor-α in human non-small cell lung cancer. Surg Oncol 1(1):49–60
54. Resat H, Ewald JA, Dixon DA, Wiley HS (2003) An integrated model of epidermal growth factor receptor trafficking and signal transduction. Biophys J 85(2):730–743
55. Ribba B, Boetsch C, Nayak T, Grimm HP, Charo J, Evers S, Teichgräber V (2018) Prediction of the optimal dosing regimen using a mathematical model of tumor uptake for immunocytokine-based cancer immunotherapy. Clin Cancer Res 24(14):3325–3333
56. Rocha HL, Almeida RC, Lima EABF, Resende ACM, Oden JT, Yankeelov TE (2018) A hybrid three-scale model of tumor growth. Mathe Mod Methods Appl Sci 28(01):61–93
57. Rosso F, Giordano A, Barbarisi M, Barbarisi A (2004) From cell–ECM interactions to tissue engineering. J Cellul Physiol 199(2):174–180
58. Rusch V, Baselga J, Cordon-Cardo C, Orazem J, Zaman M, Hoda S, … Dmitrovsky E (1993) Differential expression of the epidermal growth factor receptor and its ligands in primary non-small cell lung cancers and adjacent benign lung. Cancer Res53(10):2379–2385
59. Sadhukhan S, Mishra PK, Basu SK, Mandal JK (2021) Multiscale agent-based model for avascular tumour growth. (under review)
60. Sannino G, Marchetto A, Kirchner T, Grünewald TG (2017) Epithelial-to-mesenchymal and mesenchymal-to-epithelial transition in mesenchymal tumors: a paradox in sarcomas? Cancer Res 77(17):4556–4561
61. Santos SD, Verveer PJ, Bastiaens PI (2007) Growth factor-induced MAPK network topology shapes Erk response determining PC-12 cell fate. Nat Cell Biol 9(3):324–330
62. Sasagawa S, Ozaki YI, Fujita K, Kuroda S (2005) Prediction and validation of the distinct dynamics of transient and sustained ERK activation. Nat Cell Biol 7(4):365–373
63. Schoeberl B, Eichler-Jonsson C, Gilles ED, Müller G (2002) Computational modeling of the dynamics of the MAP kinase cascade activated by surface and internalized EGF receptors. Nat Biotechnol 20(4):370–375
64. Seiki M (2003) Membrane-type 1 matrix metalloproteinase: a key enzyme for tumor invasion. Cancer Lett 194(1):1–11
65. Sherratt JA, Gourley SA, Armstrong NJ, Painter KJ (2009) Boundedness of solutions of a non-local reaction-diffusion model for adhesion in cell aggregation and cancer invasion. Eur J Appl Mathe 20(1):123
66. Slodkowska EA, Cribier B, Peltre B, Jones DM, Carlson JA (2010) Calcifications associated with basal cell carcinoma: prevalence, characteristics, and correlations. Am J Dermatopathol 32(6):557–564
67. Storer NP, Peck SL, Gould F, Van Duyn JW, Kennedy GG (2003) Sensitivity analysis of a spatially-explicit stochastic simulation model of the evolution of resistance in Helicoverpa zea (Lepidoptera: Noctuidae) to Bt transgenic corn and cotton. J Econ Entomol 96(1):173–187
68. Vega S, Morales AV, Ocaña OH, Valdés F, Fabregat I, Nieto MA (2004) Snail blocks the cell cycle and confers resistance to cell death. Genes Dev 18(10):1131–1143
69. Vicent S, Garayoa M, López-Picazo JM, Lozano MD, Toledo G, Thunnissen FB, … Montuenga LM (2004) Mitogen-activated protein kinase phosphatase-1 is overexpressed in non-small cell lung cancer and is an independent predictor of outcome in patients. Clin Cancer Res10(11):3639–3649
70. Wang Z, Zhang L, Sagotsky J, Deisboeck TS (2007) Simulating non-small cell lung cancer with a multiscale agent-based model. Theor Biol Med Modell 4(1):50
71. Werfel J, Krause S, Bischof AG, Mannix RJ, Tobin H, Bar-Yam Y, … Ingber DE (2013) How changes in extracellular matrix mechanics and gene expression variability might combine to drive cancer progression. PLoS One 8(10):e76122
72. Wirtz D, Konstantopoulos K, Searson PC (2011) The physics of cancer: the role of physical interactions and mechanical forces in metastasis. Nat Rev Cancer 11(7):512
73. Xue C, Wyckoff J, Liang F, Sidani M, Violini S, Tsai KL, … Segall JE (2006) Epidermal growth factor receptor overexpression results in increased tumor cell motility in vivo co-ordinately with enhanced intravasation and metastasis. Cancer Res 66(1):192–197
74. Zetter BR (1998) Angiogenesis and tumor metastasis. Ann Rev Med 49(1):407–424
75. Zhang L, Athale CA, Deisboeck TS (2007) Development of a three-dimensional multiscale agent-based tumor model: simulating gene-protein interaction profiles, cell phenotypes and multicellular patterns in brain cancer. J Theor Biol 244(1):96–107

Sounak Sadhukhan, M.E. pursuing Ph.D. in Computer Science, Institute of Science, Banaras Hindu University, India. He has 7 years of research experience and has interests in biological modelling.

P. K. Mishra, Ph.D. Professor in Department of Computer Science, Institute of Science, Banaras Hindu University, India. His research interests include Data Mining, IoT, High Performance Computing, and VLSI Algorithms.